ORNL/CDIAC-160
NDP-094

Climatological Distributions of pH, pCO_2, Total CO_2, Alkalinity, and $CaCO_3$ Saturation in the Global Surface Ocean

Contributed by
Taro Takahashi, Stewart C. Sutherland, David W. Chipman, John G. Goddard
Lamont-Doherty Earth Observatory of Columbia University,
Palisades, NY 10964
and
Timothy Newberger and Colm Sweeney
Cooperative Institute in Environmental Sciences, University of Colorado,
Boulder, CO 80309

Prepared by
Alex Kozyr
Carbon Dioxide Information Analysis Center
Oak Ridge National Laboratory
Oak Ridge, Tennessee, USA

Date published: September 2014

Prepared for the Climate Change Research Division
Office of Biological and Environmental Research
U.S. Department of Energy
Budget Activity Numbers KP 12 04 01 0 and KP 12 02 03 0

Prepared by the
Carbon Dioxide Information Analysis Center
OAK RIDGE NATIONAL LABORATORY
Oak Ridge, Tennessee 37831-6335
managed by
UT-BATTELLE, LLC
for the
U.S. DEPARTMENT OF ENERGY
under contract DE-AC05-00OR2272

ABSTRACT

Takahashi, T., S. C. Sutherland, D. W. Chipman, J. G. Goddard, T. Newberger and C. Sweeney. 2014. Climatological Distributions of pH, pCO_2, Total CO_2, Alkalinity, and $CaCO_3$ Saturation in the Global Surface Ocean. ORNL/CDIAC-160, NDP-094. Carbon Dioxide Information Analysis Center, Oak Ridge National Laboratory, U.S. Department of Energy, Oak Ridge, Tennessee. doi: 10.3334/CDIAC/OTG.NDP094

Climatological mean monthly distributions of pH in the total H^+ scale, total CO_2 concentration (TCO_2), and the degree of $CaCO_3$ saturation for the global surface ocean waters (excluding coastal areas) are calculated using a data set for pCO_2, alkalinity and nutrient concentrations in surface waters (depths <50 m), which is built upon the GLODAP, CARINA and LDEO database. The mutual consistency among these measured parameters is demonstrated using the inorganic carbon chemistry model with the dissociation constants for carbonic acid by Lueker et al. (2000) and for boric acid by Dickson (1990). The global ocean is divided into 24 regions, and the linear potential alkalinity-salinity relationships are established for each region. The mean monthly distributions of pH and carbon chemistry parameters for the reference year 2005 are computed using the climatological mean monthly pCO_2 data adjusted to a reference year 2005 and the alkalinity estimated from the potential alkalinity-salinity relationships. The equatorial zone (4°N-4°S) of the Pacific is excluded from the analysis because of the large interannual changes. The pH thus calculated ranges from 7.9 to 8.2. Lower values are located in the upwelling regions in the tropical Pacific and in the Arabian and Bering Seas; and higher values are found in the subpolar and polar waters during the spring-summer months of intense photosynthetic production. The vast areas of subtropical oceans have seasonally varying pH values ranging from 8.05 during warmer months to 8.15 during colder months. The warm tropical and subtropical waters are supersaturated by a factor of as much as 4.2 with respect to aragonite and 6.3 for calcite, whereas the cold subpolar and polar waters are less supersaturated only by 1.2 for aragonite and 2 for calcite because of the lower pH values resulting from greater TCO_2 concentrations. In the western Arctic Ocean, aragonite undersaturation is observed. This report describes the data assembled for the study and the methods used for the computation of the pH, TCO_2, and degree of saturation of $CaCO_3$ in global ocean surface waters.

1. INTRODUCTION

Most active biological production takes place in the sun-lit top layer of the global ocean. Yet, this is the layer that is being acidified as a result of the absorption of rapidly increasing CO_2 from the atmosphere. Many biogeochemical reactions in general will be influenced by changes in ocean water pH: especially, calcifying organisms such as corals, foraminifera, pteropods and coccolithophores will be impacted directly due to the reduced degree of saturation of $CaCO_3$ in seawater (Feely et al., 2012). At several time series stations such as BATS (Bermuda Atlantic Time series Study) (Bates et al., 1996; Bates, 2007; Bates et al., 2012), HOT (Hawaii Ocean Time-series) (Dore et al., 2003; Dore et al., 2009), ESTOC (European Station for Time series in the Ocean Canary Islands) (Gonzalez-Dávila et al., 2003; Gonzalez-Dávila et al., 2007; Santana-Casiano et al., 2007; Gonzalez-Dávila et al., 2010) and Iceland Sea (Olafsson et al., 2009), the acidification of seawater has been documented for the past decades. The present pH conditions and future acidification of the global ocean waters by the ocean uptake of CO_2 have been reviewed by Feely et al. (2009) using a biogeochemical ocean GCM. More locally, the rapid acidification in the California Current system has been extensively investigated by Gruber et al. (2012) and Hauri et al. (2013) using a dynamic ocean circulation model combined with the multi-year observations. All of these studies indicate a significant degree of acidification in the surface ocean waters. However, although pH and its change have been measured at many study sites and during cruises using various pH sensor systems, the data are not globally comparable because of calibration problems and methodological differences associated with the pH measurements (Marion et al., 2011). Presently, the global distribution of ocean water pH is based on Biogeochemical Ocean General Circulation Models (BOGCM) (e.g. Orr et al., 2005; Doney et al., 2009; Feely et al., 2009) which include limited descriptions of marine ecosystems and community productions, but without land-ocean interactions. An observation-based global ocean pH distribution is desired for establishing a baseline for the future changes in oceanic carbonate chemistry, thus placing the ocean acidification study on a firmer ground.

The objective of this study is to obtain the climatological mean distribution of pH and associated carbon chemistry properties in global surface ocean waters with a single unified scale for the calculated pH. These properties will be computed on the basis of the observations made for CO_2 partial pressure (pCO_2), total alkalinity (TALK) and total CO_2 concentration (TCO_2) in surface waters ($Z<50$ m). It is imperative that these observations are based on common standards which are stable over many decades to insure the compatibility of the data in space and time. In Section 2, the principles for the method employed in this study will be briefly explained. In Section 3, the potential alkalinity (PALK = TALK + nitrate) - salinity relationships observed in 24 oceanic regions will be

presented. The mean monthly distributions of TALK and pCO_2 in surface waters of the global ocean in a 4° x 5° spatial resolution, which will be used for computing pH and other carbon chemistry properties, will be shown. In Section 4, the computed results are tested against the observations made at various locations including the BATS, HOT and ESTOC sites, and the limitations for the method used for this study are discussed. In Section 5, the climatological distribution of pH, degree of $CaCO_3$ saturation and TCO_2 in the global ocean will be presented. The database and results described in this report are used in the published paper by Takahashi et al. (2014).

2. PRINCIPLES

The concentrations of H^+ (or pH) and $CO_3^=$ ions and the degree of saturation for calcite and aragonite in seawater may be computed using an inorganic equilibrium model for carbonate chemistry in seawater when temperature, salinity, pCO_2, TCO_2 or the total alkalinity are measured. The most desirable way for computing pH and carbonate chemistry parameters is to use pCO_2 and TCO_2 for two reasons: a) both pCO_2 and TCO_2 measurements share the well-established air-CO_2 gas mixture standards (e. g. Keeling, 1960 and the NOAA Earth System Research Laboratory, Boulder, CO); and b) the solubility of CO_2 and dissociation constants for carbonic acid in seawater are the only information needed. However, seasonal variability for pCO_2 and TCO_2 is large due to seasonal changes in SST, net community production and upwelling of deep waters. While seasonal variability data for pCO_2 are available for many locations in the global oceans (e.g. Takahashi et al., 2009; Takahashi et al, 2013), the TCO_2 observations are too few to define seasonal changes other than those obtained at a few time-series stations. Hence, the TCO_2 data are not sufficient for establishing the global distribution of pH and other carbonate chemistry parameters, although the available data may be used for testing and validating the internal consistency of our analysis method.

The carbonate chemistry in seawater may be also defined using a combination of pCO_2 and the total alkalinity (TALK). However, this scheme requires additional measurements for the concentrations of boric, phosphoric and silicic acids as well as the dissociation constants for each acid species, in order to correct for the contribution of these weak acids to the TALK. While the errors are negligibly small for the low nutrient subtropical gyre waters, the errors may be large for high nutrient waters in high latitude and upwelling areas. Surface water TALK is governed primarily by a) water balance (i.e. evaporation - precipitation), b) upwelling of high alkalinity deep waters (due to the dissolution of $CaCO_3$), c) production of $CaCO_3$ shells within the mixed layer and d) mixing between waters with different characteristics. Since the vertical gradient for TALK in the upper five hundred meters of water column is much smaller (1/2 to 1/10) than that for TCO_2, and since the biological production of $CaCO_3$ shells is commonly less than 1/10 the net community production of organic carbon (with the exception of the coccolithophore blooms (Balch et al., 2005)), TALK in surface water is primarily related to salinity, and the TALK values normalized to a constant salinity are found to be seasonally invariant in the low nutrient oligotrophic waters (e. g. Bates et al., 1996; Bates, 2001). On the other hand, TALK depends also on the concentration of NO_3^- (and to small extent on phosphate), which varies seasonally between 0 and 30 μmol kg^{-1} (e. g. Takahashi et al., 1993; Hales and Takahashi, 2004) in high latitude waters due to deep water upwelling and biological utilization. Accordingly, TALK may be altered

seasonally by as much as 30 μeq kg^{-1}. We, therefore, look for the salinity dependence of the potential alkalinity (PALK = TALK + NO_3^-, Brewer and Goldman, 1976), which compensates for the effect of change in NO_3^-. An advantage of this scheme is that the seasonal variability of PALK is generally small, and the seasonal change in TALK caused by nutrient change may be explicitly estimated from the salinity and nitrate data in a specific region. The observed regional differences in the PALK - salinity relationships reflect primarily changes in $CaCO_3$ production in surface waters and mixing with high TALK deep waters produced by the dissolution of $CaCO_3$.

Our approach for estimating TALK is in contrast to the previous work by Millero et al. (1998) and Lee et al. (2006), who parameterized TALK as a function of salinity and SST without including parameter(s) representing explicitly the net community production. In their formulations, SST was used as a proxy for the combined effect of complex seasonal processes including net community production, $CaCO_3$ formation and lateral/vertical mixing. In our study, the TALK change caused by seasonal net community production is corrected using seasonal NO_3^- data. The results of these studies will be compared with this study in Section 3.3.1.

In this report, the climatological distributions for pH (in the total H^+ scale), $CO_3^=$ and other related values in a 4° x 5° grid are computed with an inorganic carbonate chemistry model using the climatological mean values for surface water pCO_2 for the reference year 2005 (an up-dated version of Takahashi et al., 2009), total alkalinity, salinity and temperature. In order to demonstrate the global integrity of the computed pH and other values, TCO_2 values which are computed from the pCO_2-TALK data with the chemical model are compared with the available TCO_2 data. As shown in Section 4, the computed values are found to be consistent with the observed values, with a few exceptions attributable to the relatively coarse 4° x 5° spatial resolution used in this study. The equilibrium carbon chemistry model consists of the following dissociation constants and CO_2 solubility in seawater: Lueker et al. (2000) for carbonic acid, Dickson (1990) for boric acid, Dickson and Riley (1979-a) for water, Dickson and Riley (1979-b) for phosphoric acid, Sjorberg et al. (1981) for silicic acid and Weiss (1974) for the CO_2 solubility. The dissociation constants for carbonic acid by Lueker et al. (2000) are selected because (a) the experiments are conducted by measuring all four variables (pCO_2, TCO_2, alkalinity and pH) in natural seawater samples, and (b) the pCO_2 and TCO_2 are determined using the manometric standards established by Keeling (1960) and the NOAA Earth System Research Laboratory, that are also used for the field observations used in this study. In this model, the total H^+ ion scale (concentrations of free H^+ plus HSO_4^- ions (Dickson, 1993)) is used, and the effects of organic acids are not included. The degree of saturation for calcite and aragonite are computed using the apparent solubility products (Ksp') of Mucci (1983).

3. OBSERVATIONS AND ANALYSIS

The availability of the observations needed for this study varies widely in each parameter. While about 6 million pCO_2 data are available for the various seasons since 1950's over the global oceans (Takahashi et al., 2013), there are only about 16,000 TCO_2 and alkalinity measurements which are mostly limited to summer time since 1980's. In only 2,200 of them, pCO_2, TCO_2 and TALK have been measured in the same samples.

We will first test the mutual consistency of these three properties using this set of data and the chemical model described in Section 2. Once this is confirmed, then the global distribution of pH, TCO_2 and other carbon chemistry parameters will be computed using the climatological mean monthly distribution of pCO_2 and the alkalinity estimated using the characteristic PALK-salinity relationships found in various ocean regions. The observed TCO_2 values will be compared with the calculated values for the validation of the method.

3.1. The TALK-TCO_2-pCO_2 Database:

We assembled a carbon-nutrient database (named LDEO_SurCarbChem) for the upper 50 meters of ocean water measured during the TTO, SAVE, WOCE and CARINA programs. This database, which is described in this report, is built upon the data synthesis of the GLODAP database (Key et al., 2004), and also includes the TCO_2-TALK pairs from the CARINA program (Tanhua et al., 2009; Key et al., 2010) and pCO_2 and TCO_2 data from the LDEO database (also available to the public at the Biological and Chemical Oceanography Data Management Office (BCO-DMO), Woods Hole Oceanographic Institution). The pCO_2 data are based on the air-CO_2 gas mixture standards certified by Pieter Tans of NOAA Earth System Research Laboratory (ESRL), and the TCO_2 data are consistent with the CO_2 reference solutions prepared by Dickson (2001), which are based on the Keeling CO_2 standards (which are consistent with the NOAA/ESRL values). Of about 16,000 records listed in this database, about 4,800 records are from the CARINA database, and 2,600 pCO_2 data are from LDEO database. Several thousand TCO_2 measurements made by the LDEO group are already included in the GLODAP database. Of these, 2,205 sets have the pCO_2, TCO_2 and TALK in the same samples. The mutual consistency between these three parameters in this subset is tested by comparing computed values with measured values (Figure 1). The calculated values are found to be consistent with the measured values within the measurement uncertainties respectively: the TALK values computed using pCO_2 and TCO_2 as inputs are in agreement with the measured values with a root mean square deviation (RMSD) of $\pm$ 3.9 μeq kg^{-1}; the computed TCO_2 values from the pCO_2 and alkalinity data are in agreement with the measured values with $\pm$ 3.3 μmol kg^{-1}; and the computed pCO_2 values from the TCO_2 and TALK data are in agreement with the measured values with $\pm$6.8 μatm. This demonstrates that these three properties are mutually consistent within the context of the equilibrium model, and that one property may be computed reliably when two others are given.

Figure 1 – Comparison of the observed values with the calculated values from the pCO_2, TCO_2 and alkalinity data for 2,205 sets of observations in surface waters. The black line shows the linear regression line, and the red crosses and the red right-hand axis indicate the deviations around the regression line. (Top) The calculated TALK values using pCO_2 and TCO_2 are in agreement with the measured values within RMSD of $\pm$ 3.9 μeq kg^{-1}; (Middle) the calculated TCO_2 values using pCO_2 and alkalinity are in agreement with the measured values within RMSD of $\pm$ 3.3 μmol kg^{-1}; and (Bottom) the calculated pCO_2 values using TCO_2 and TALK are in agreement with the measured values within $\pm$ 6.8 μatm.

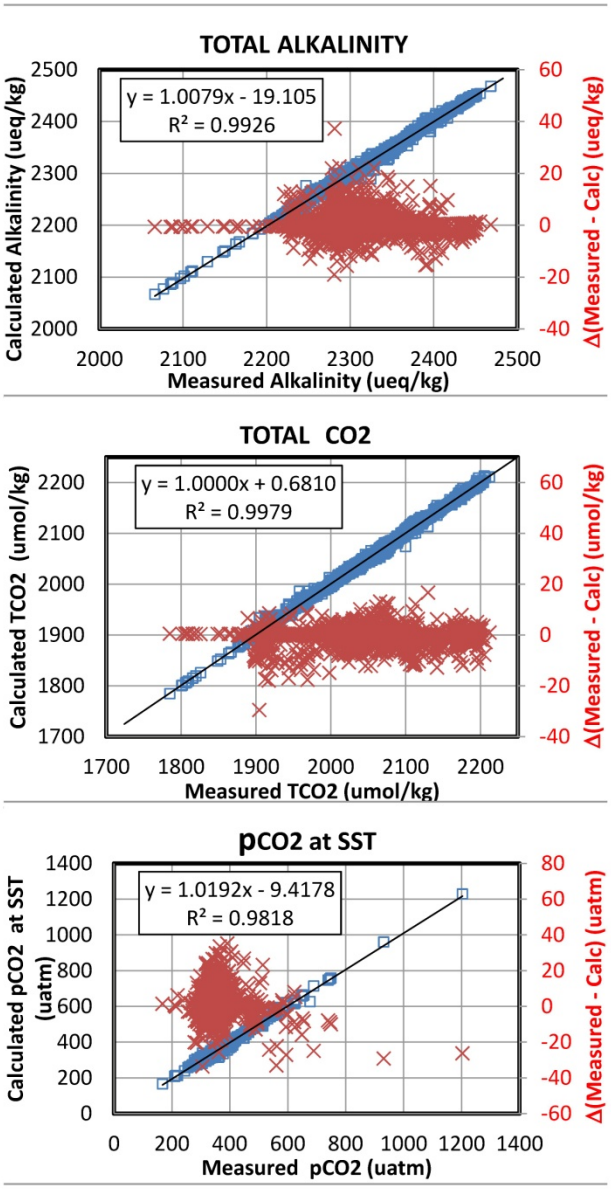

3.2 Potential Alkalinity-Salinity Relationships:

We use the "LDEO SurfCarbChem" database described above, and demonstrate that the PALK varies linearly with salinity within respective oceanic regions. The value of TALK, which is needed for the carbonate chemistry calculation, is estimated using the PALK-salinity relationship and the NO_3^- data. The PALK-salinity relationship depends primarily on the evaporation-precipitation (E-P*)* of water, the formation and dissolution of $CaCO_3$ as well as mixing with waters of different characteristics (including river and deep waters). Five different cases showing how the slope of the linear PALK-salinity relationships varies with different oceanographic situations are illustrated in Figure 2.

Figure 2 – Variations of the potential alkalinity-salinity relationships. The effect of evaporation and precipitation is indicated by the light solid line. The slope of the line is altered by the production/dissolution of $CaCO_3$, upwelling of deep waters, mixing with river waters, and mixing with seawaters with different compositions.

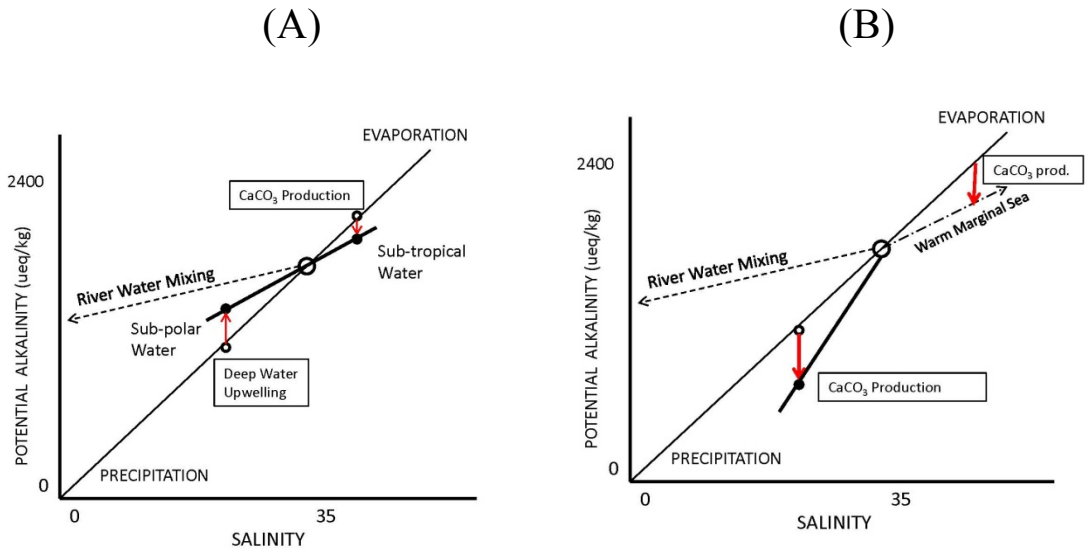

---

(1) The change of PALK due to the evaporateon-precipitation (E-P) of water is depicted by a straight line passing through the origin and the source water (heavy open circle in Figures 2-A and-B). An example is found in the Central Tropical North Pacific region in Figure 5 (green line).

(2) As shown in Figure 2-A, subtropical waters that have higher salinity and reduced PALK due to the growth of calcareous organisms (downward red arrow in the left panel) are represented by the small filled circle: in contrast, subpolar waters that are less salty and enriched in PALK due to deep water upwelling (small filled circle with a upward red arrow). The mixing line between these two water types (the heavy straight line) has a shallower slope than the E-P line. This type of relationships is commonly observed in the subtropical gyres in the Atlantic (Figure 4), Pacific (Figures 5 and 6) and Indian Ocean (Figures 7 and 8), and is represented by the positive intercept values in regression lines (summarized in Table 1).

(3) Figure 2-B shows the case when PALK in lower salinity waters is reduced by the growth of calcareous organisms. The mixing line for this case has a slope steeper than the E-P line. Such a case is found in the Panama Basin (Figure 5, red line), which is represented by a negative intercept value in the regression line (Table 1).

(4) The source water may be mixed with river water that has a higher PALK value as shown by the dashed line in Figures 2-A and -B. River waters are commonly fresh and contain PALK derived from the dissolution of limestones. This type of relationships is found in the Okhotsk Sea (black line in Figure 5) and the Bengal Basin (red line in Figure 7), which also have positive intercept values for regression lines (Table 1).

(5) The source water may be also mixed with waters which have high salinity and reduced PALK (marked Warm Marginal Sea in Figure 2-B). Such a trend may be found for the mixing with an outflow from a warm evaporative basin like the Red Sea (green line in Figure 7).

The characteristic linear PALK-salinity relationships are observed in 27 ocean regions, and they are presented in Figures 3 through 9. However, the relationships in six regions can not be described satisfactorily using linear equations because of time-space variation of complex mixing of various water types: the subtropical-subarctic transition zones due to intense eddy mixing, and the Pacific equatorial belt affected by El Niño events due to reorganization of ocean dynamics (Feely et al., 2002). These zones are indicated with the tangerine color in the sample distribution maps of Figures 4 - 8, and are marked with special symbols in our maps. The linear regression equations and root mean square deviations (RMSD) are summarized in Table 1. Of the 33 regions listed in Table 1, five regions which are marked "Transition Zone" and one marked "El Niño Zone" are excluded from further analysis. In addition, the three Southern Ocean regions for the Atlantic, Indian and Pacific sectors are combined together as a single Circumpolar Southern Ocean region (see Section 3.2.7). The remaining 24 regions have the RMSD values ranging between ± 4 and ± 17 μeq kg^{-1} with a mean RMSD of ± 8.2 μeq kg^{-1} (excluding ± 60.5 μeq kg^{-1} for the Beaufort Sea, Table 1), and are used in this study. The level of deviations is considered acceptable in comparison with the precision of ± 6 μeq kg^{-1} estimated for the PALK measurements. A few regions with large RMSD will be commented in the respective sections below.

Table 1 –The potential alkalinity-salinity relationships in 33 ocean areas. Five regions which are marked "Transition Zone" and one marked "El Niño Zone" are excluded from the analysis. The Atlantic, Indian and Pacific sectors of the Southern Ocean are combined together as a single Circumpolar Southern Ocean region (see Section 3.2.7). The remaining 24 regions are used in producing the climatological distributions of TALK. PALK (μeq kg^{-1}) = (Slope) x (Salinity, PSS) + Intercept (μeq kg^{-1}), and RMSD = Root mean square deviation (μeq kg^{-1}).

	REGIONS	LOCATIONS	REGRESSION EQUATIONS			BOX AREAS
			Slope	Intercept	RMSD	
	ARCTIC & GIN SEAS					
1	West GIN Seas	66°N - 80°N, 30°W - 0°	14.12	1796.2	6.1	68N-76N, 332.5 to 357.5
2	East GIN Seas	66°N - 80°N, 0° - 30°E	59.57	232.0	12.3	68N-76N, 2.5 to 32.5
3	High Arctic	N of 80°N	27.30	1340.7	16.8	80N-88N, 2.5 to 357.5
4	Beaufort Sea	66°N - 80°N, 140°W - 180°	61.29	285.8	60.5	68N-76N, 180 to 222.5
5	Labrador Sea	55°N - 80°N, 85°W - 45°W	37.27	1016.2	17.2	56N-76N, 277.5 to 312.5
6	Subarctic Atlantic	55°N - 80°N, 40°W - 10°E	45.37	730.6	6.7	56N-76N, 317.5 to 7.5
	NORTH & SOUTH ATLANTIC OCEAN					
7	N. Atlantic Drift	40°N - 55°N, 60°W - 10°E	45.30	733.0	6.5	44N-52N, 302.5 to 7.5
8	Central Atlantic	40°S - 40°N, Coast to Coast	58.25	270.9	12.6	40S-40N, Ocean width
9	S. Atlantic Transition Zone	40°S - 48°S, 65°W - 30°E	30.27	1259.4	7.6	44S-48S, 297.5 to 27.5
10	S. Atlantic Subpolar Front Zone	48°S - 60°S. 70°W - 30°E		Transition Zone		48S-56S, 292.5 to 27.5
11	Antarctic (Atlantic)	60°S - 70°S, 70°W - 30°E	57.78	367.8	5.4	60S-68S, 292.5 to 27.5
	NORTH & SOUTH PACIFIC OCEAN					
12	Kuroshio-Alaska Gyre	34°N - 40°N, Ocean width & N of 40°N, E of 150°W	44.88	724.8	9.0	36N , Ocean width 40N-60N, 107.5 to 207.5
13	N. Central Pacific	44°N - 60°N, W of 150°W	79.92	-395.7	14.7	44N-56N, 207.5 to 237.5
14	N. Pacific Subpolar Front Zone	40°N - 44°N, 140°E - 145°W		Transition Zone		40N-44N, 137.5 to 217.5
15	Okhotsk Sea	47°N - 60°N, W of 152°E	59.37	301.4	8.9	48N-60N, 122.5 to 152.5
16	N. Pacific Subtropical Front Zone	30°N - 34°N, 130°E - 120°W		Transition Zone		32N, 142.5 to 242.5
17	Central Tropical N. Pacific	5°N - 30°N, W of 120°W	65.55	9.4	8.9	8N-28N, 107.5 to 122.5
18	Tropical East N. Pacific	5°N - 30°N, 120°W - 95°W	82.20	-553.2	9.7	8N-28N, 127.5 to 262.5
19	Panama Basin	0°N - 15°N, 95°W - 80°W	74.27	-290.5	8.6	8N-12N, 267.5 to 282.5
20	Equatorial Pacific	5°S - 5°N, 130°E - 80°W		El Nino Zone		4S-4N, 127.5 to 277.5
21	Central South Pacific	5°S - 35°S. 150°E - 84°W	66.64	-28.4	9.4	8S-36S, 142.5 to 277.5
22	E. Central South Pacific	5°S - 60°S, E of 84°W	58.88	268.5	4.0	8S-56S, 282.5 to 307.5
23	Subpolar S. Pacific	35°S - 50°S, 180° - 84°W	45.10	733.6	7.8	34S-48S, 180 to 277.5
24	S. Pacific Subpolar Front Zone	50°S - 65°S, 150°E - 70°W		Transition Zone		52S-58S, 152.5 to 297.5
25	Antarctic (Pacific)	65°S - 75°S, 140°E - 65°W	81.69	-450.8	6.7	64S-80S, 137.5 to 292.5
	NORTH & SOUTH INDIAN OCEAN					
26	Main North Indian	5°N - 25°N, 48°E - 100°E	57.07	302.3	6.7	4N-24N, 47.5 to 102.5
27	Red Sea	12°N - 27°N, 34°E - 48°E	26.27	1417.2	6.3	12N-24N, 32.5 to 47.5
28	Bengal Basin	10°N - 20°N, 80°E - 100°E	39.66	894.2	10.7	12N-24N, 77.5 to 102.5
29	Main South Indian	5°N - 40°S. 30°E - 140°E	65.03	20.0	7.6	4N-36S, 27.5 to 142.5
30	S. Indian Transition	40°S - 48°S, 30°E - 175°E	23.76	1486.1	5.5	40S-48S, 27.5 to 172.5
32	S. Indian Subpolar Front Zone	48°S - 52°S, 30°E - 150°E		Transition Zone		Overlap above & below
32	Antarctic (Indian)	52°S - 70°S, 25°E - 165°E	62.57	202.0	6.6	52S-68S, 22.5 to 167.5
	SOUTHERN OCEAN					
33	Circumpolar Southern Ocean	S of 60°S, All Southern	74.13	-192.3	9.1	60S-84S, 2.5 to 357.5

3.2.1 Arctic-GIN Seas (north of 55°N):

Figure 3 shows the data locations (upper left map) and the PALK data (lower left) in the Arctic and Greenland-Iceland-Norwegian (GIN) Seas. The GIN Seas are divided into two areas: the western half, which represents primarily the waters flowing out of the Arctic (including the East Greenland Current), and the eastern half, which represents the Atlantic waters flowing northward into the Arctic basin. The data and linear regression line for each of the six regions are shown in the plots on the right. The large RMSD of 60 $\mu eq\ kg^{-1}$ in the Beaufort Sea (red plot, top right) is due to complex coastal shelf processes occurring in shallow waters comprising of the river, Arctic and Pacific sources (Anderson et al., 2004; Bates and Mathis, 2009). The high values found in the High Arctic and Labrador Sea (RMSD of 16.8 $\mu eq\ kg^{-1}$ and 17.2 $\mu eq\ kg^{-1}$ respectively) are also due to complex mixing of river, ocean and ice-melt waters. Until more high-resolution data become available in the future, these regression lines are accepted in this study as the best representation of the available data.

Figure 3 - Sample locations (upper left) and the potential alkalinity (PALK)-salinity relationships in the Arctic and GIN Seas. All observations are shown in the lower left plot. The data are binned into the six regions: black = Western GIN Seas (66°N-80°N, 30°W-0°), cyan = Eastern GIN Seas (66°N-80°N, 0°-30°E), magenta = high Arctic (N of 80°N), red = Beaufort Sea (66°N-80°N, 140°W-180°), green = Labrador Sea (55°N-80°N, 85°W-45°W) and blue = Subarctic Atlantic drift (66°N-80°N, 40°W-10°E). The same color code is used for the PALK-salinity plots (middle and right rows), in which linear regression lines and respective equations are shown. In the West GIN Sea plot, two lines are drawn: the cyan line is the regression line for the East GIN Sea data (shown in the plot below), and the black line is the regression line for the data excluding the points, that appear to belong to eddies from the East GIN Sea side.

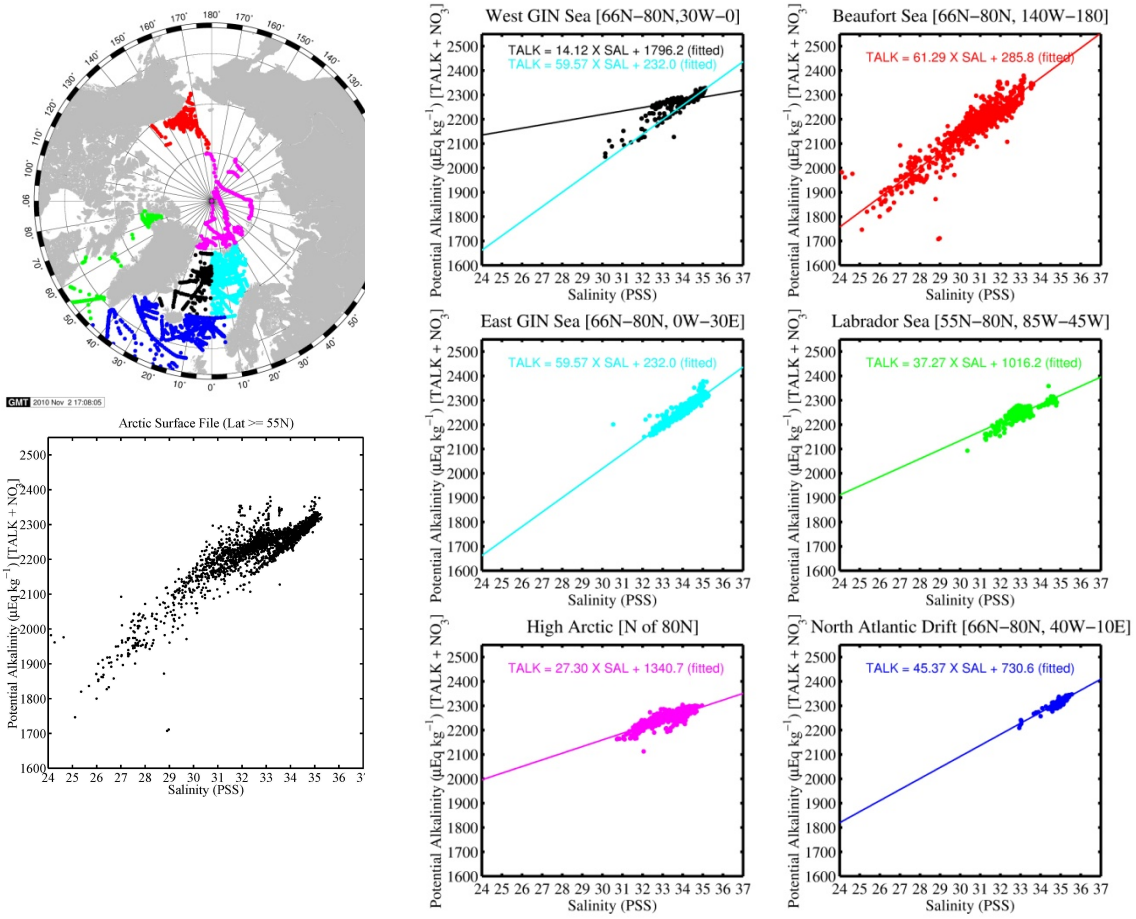

3.2.2 Atlantic Ocean (55°N – 70°S):

The PALK-salinity relationships in the North and South Atlantic Ocean are shown in Figure 4. The map on the left shows the sample locations, and the black plot on the top center shows the entire data set. The North Atlantic drift waters (40°N - 55°N) exhibit a tight linear correlation (upper right, cyan plot), and have greater PALK values than the tropical and subtropical regions by 10 to 50 μeq kg^{-1}. This may be attributed to the upwelling of deep waters as well as to the mixing of the high-alkalinity low-salinity Arctic waters. The regression line for the drift coincides closely with that for the sub-Arctic Atlantic region (Figure 3) as both regions are located within the subpolar gyre. The PALK distribution in the large expanse of the subtropical and tropical Atlantic Ocean between 40°N and 40°S may be characterized with a single linear regression line (blue plot) with a RMSD value of ± 12.6 μeq kg^{-1}. Although the subtropical South Atlantic waters tend to have somewhat lower PALK values, they are statistically indistinguishable from the northern subtropical waters. For this reason, the north and south subtropical waters are combined to yield a single regression line. In the sub-Antarctic transition zone (tangerine in the map), the PALK values vary in space and time, and no systematic trend is found. The Southern Ocean waters (red plot) have about 100 μeq kg^{-1} greater PALK than the subtropical waters. This may be also accounted for by

the more intense vertical mixing in the Southern Ocean. The mean RMSD for the four regions is ± 8.0 μeq kg^{-1}.

Figure 4 – The North and South Atlantic Ocean is divided into five regions as shown in the map (left): cyan = North Atlantic drift region (40°N-55°N, 60°W-10°E), blue = main central Atlantic (40°N – 40°S), green = Southern transition zone (40°S-48°S, 60°W-30°E), tangerine = highly variable zone (48°S-60°S, 60°W-30°E) and red = Southern Ocean (60°S-70°S, 70°W-30°E). All data in the map areas are shown in the top center plot (black), and the data and the linear regression lines in four regions are shown in the plots (right) with the same color code as in the map. Since the data in the tangerine region are highly variable in space and time, the data and regression line in this region are not used in the analysis.

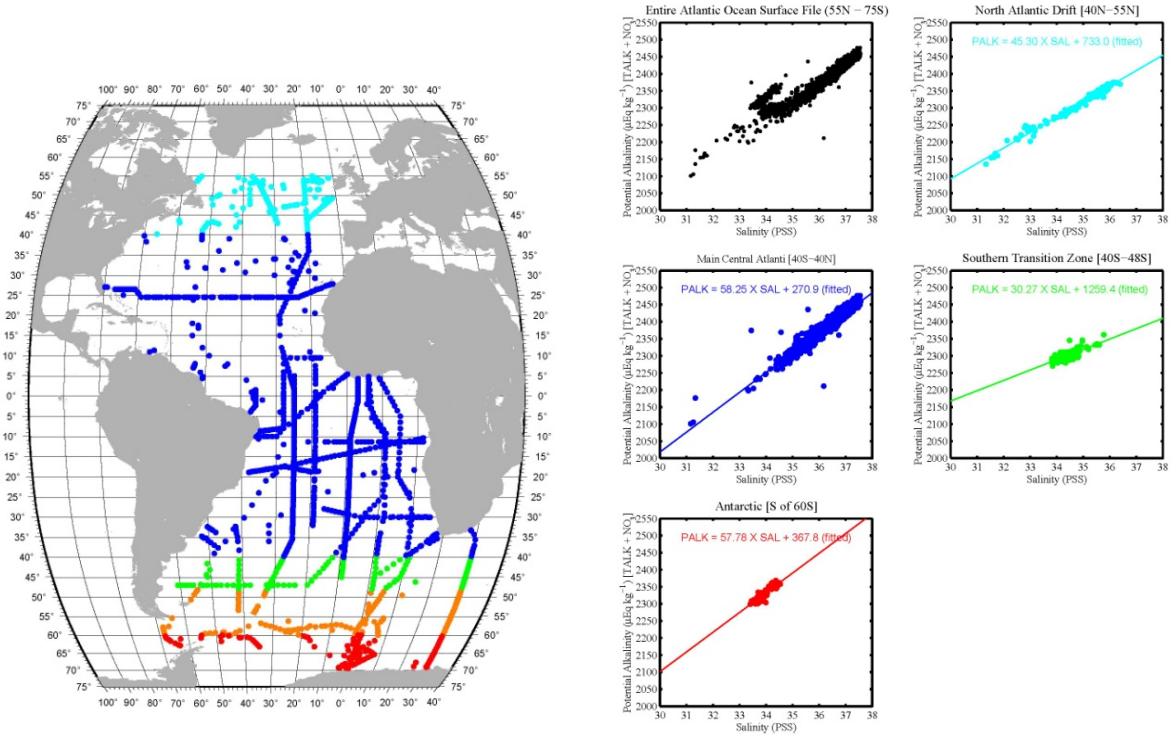

3.2.3 North Pacific Ocean (60°N – the equator):

The six divisions in the North Pacific Ocean are shown in Figure 5 (top left map), and the PALK-salinity relationship in the entire North Pacific is presented in the plot in the top right corner. Below them, shown are six colored plots for each of these six regions: the Okhotsk Sea (black). North Central-Bering Sea (magenta), Kuroshio-Alaska Gyre (blue), Central Tropical N. Pacific (green), Tropical East N. Pacific (cyan) and Panama Basin (red). The linear regression line and equation are shown in each of the six panels, and their colors coincide with the colors in the location map in Figure 5. The data from the tangerine areas are excluded from the analysis because of large interannual and spatial variability in the equatorial belt (i. e. El Niño) and in the northern and southern edges of the Kuroshio-North Pacific Current. The linear regression equations describing

the PALK-salinity relationships in the six regions of the North Pacific are summarized in Table 1, and all of them have a mean RMSD of about ± 10 μeq kg^{-1}.

Figure 5 – Map (top left) shows the sample locations for the six areas in the North Pacific, where the PALK-salinity relationships are analyzed. The top right plot shows the entire data in the North Pacific (the equator-60°N), and the lower panels show the data and regression lines in the six regions: black = Okhotsk Sea, magenta = North Central-Bering Sea (44°N-60°N, 150°E-150°W), blue = Kuroshio-Alaska Gyre (34°N-40°N,135°E-150°W and 34°N-60°N, 150°W-125°W), green = Central Tropical N. Pacific (5°N-30°N, 120°W-120°E), cyan = Tropical East N. Pacific (5°N-30°N, 95°W-120°W) and red = Panama Basin (15N-the equator, E of 95°W). The linear regression line and equation are shown in each of the six panels, and their colors coincide with the colors in the location map. The data from the tangerine areas are excluded from the analysis because of large interannual and spatial variability.

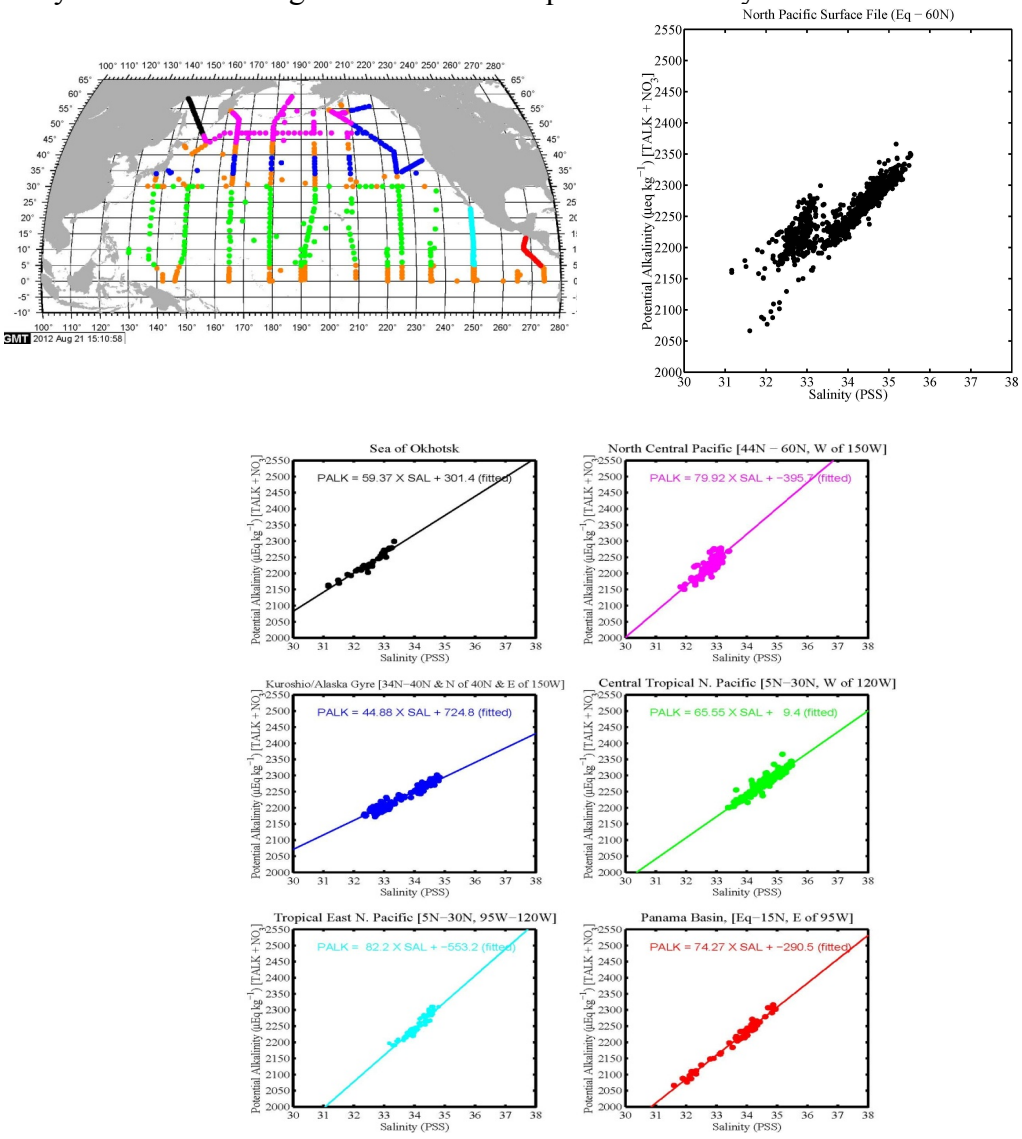

3.2.4 South Pacific Ocean (the equator-60°S):

The South Pacific (including the Pacific sector of the Southern Ocean) is divided into five regions for the PALK-salinity analysis (Figure 6). A subpolar region between 50°S-60°S (tangerine color) is excluded from the analysis because of large spatial and seasonal variability. The subtropical region (green) yields a linear regression line nearly consistent with the E-P line with a small intercept of 28.4 μeq kg^{-1} (Table 1). The waters in the eastern South Pacific (blue) and in the sub-Antarctic zone (magenta) yield large positive intercept values (Table 1) due to the addition of the low-salinity high-PALK waters from the Peru upwelling zone and the Southern Ocean. The mean RMSD for the four regions is ± 7.0 μeq kg^{-1}.

Figure 6 – Map (top center) shows the locations for the PALK-salinity data for the four areas in the South Pacific including the Southern Ocean. The top left plot (black) shows the entire data in the South Pacific (the equator-60°N), and the other panels show the data and regression lines in the four regions: green = Central South Pacific (5°S-35°S, 84°W-150°E), blue = East Central South Pacific (5°S-60°S, E of 84°W), magenta = Subpolar South Pacific (35°S-50°S, 84°W-180°), and red = Antarctic (Pacific Sector) (65°S-75°S, 65°W-140°E). The data from the tangerine areas are excluded from the analysis because of large interannual and spatial variability. The regression equations are listed in Table 1.

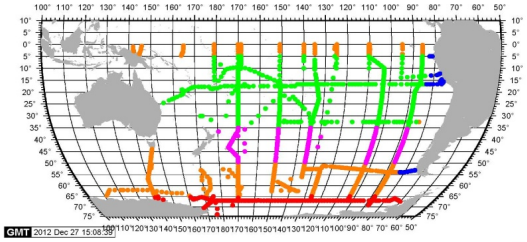

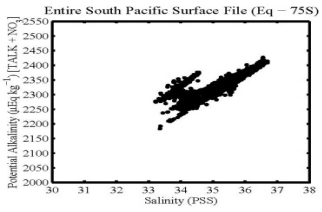

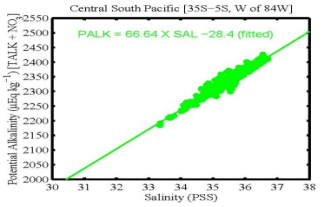

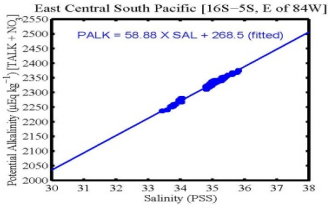

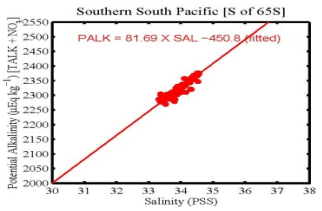

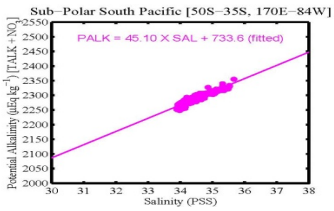

3.2.5 North Indian Ocean: (5° N – 27°N):

The North Indian Ocean is divided into three regions, and the sample locations and data are shown in Figure 7. All three regions exhibit shallower slopes than the E-P line with positive intercepts (Table 1). The positive intercept found for the Main North Indian region may be attributed to $CaCO_3$ production in high salinity waters as well as to the input of the fresh Indus River waters with additional PALK. The large positive intercept observed for the Red Sea is due to intense evaporation (high salinity) coupled with $CaCO_3$ production. The Bengal Basin trend is primarily due to the influx of the high PALK Ganges-Brahmaputra river waters. The regression equations are listed in Table 1, and the mean RMSD for these three regions is ± 7.9 μeq kg^{-1}.

Figure 7 –Map (top center) shows the locations for the PALK-salinity data for the three areas in the North Indian Ocean (5°N – 27°N) including the Red Sea. The top left plot (black) shows the entire data in the region, and the other panels show the data and regression lines in the three areas: blue = Main North Indian Ocean (25°N (10°N)-5°N, 48°E-100°E), green = Red Sea (12°N-27°N, 34°E-48°E), and red = Bengal Basin (10°N-20°N, 80°E-100°E). Note that the salinity axis is expanded to 41 because of the high salinity waters of the Red Sea. The regression equations are listed in Table 1.

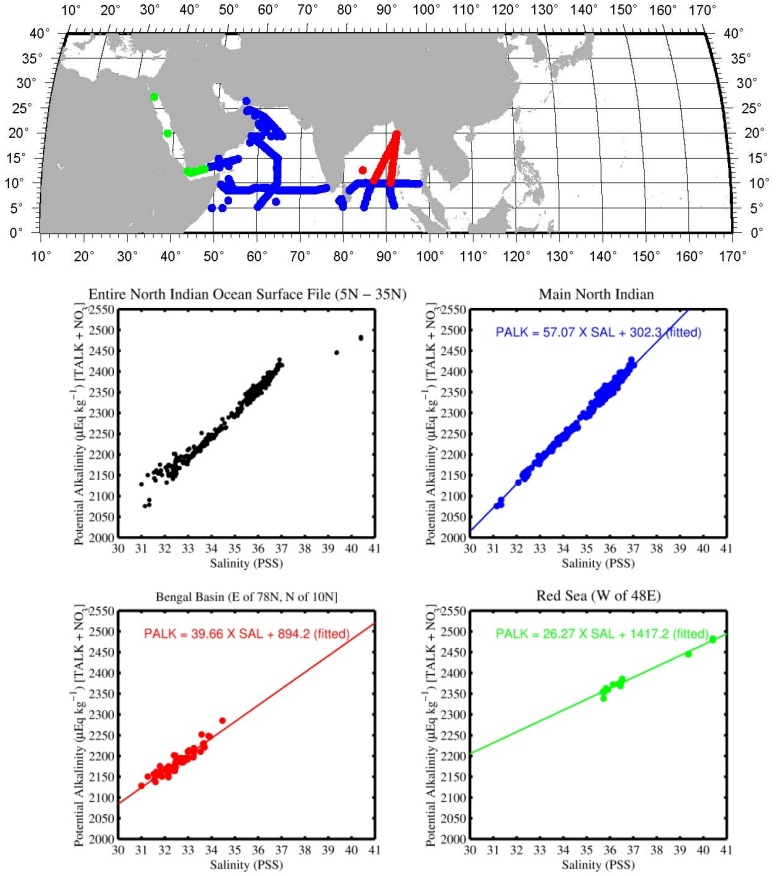

3.2.6 South Indian Ocean: (5° N – 70°S):

The South Indian Ocean is divided into four regions (Figure 8). The PALK-salinity trend (blue plot) for the Main South Indian Ocean region (5°N-40°S), which covers the subtropical and tropical oceans, has a slope nearly equal to the E-P slope, but with a small positive intercept reflecting the $CaCO_3$ production. The Southern Ocean water has about 100 μeq/kg greater PALK than the subtropical and tropical waters, due to the upwelling of the deep waters in the Southern Ocean. The flat trend (green plot) for the South Indian Transition zone represents a mixing line between the subtropical and Southern Ocean waters. The mean RMSD for the three regions is ± 6.5 μeq kg^{-1}.

Figure 8 - Map (top center) shows the locations for the PALK-salinity data for the four regions in the South Indian Ocean (5°N – 70°S). The top left plot (black) shows the entire data in the South Indian Ocean, and the other three panels show the data and regression lines in the three regions: blue = Main South Indian Ocean (5°N-40°S, 30°E-140°E), green = South Indian Transition (40°S-48°S, 30°E-150°E), and red = Antarctic (Indian Sector) (52°S-70°S, 25°E-165°E). The data from the tangerine areas (48°S-52°S) are excluded from the analysis because of large interannual and spatial variability. The regression equations are listed in Table 1.

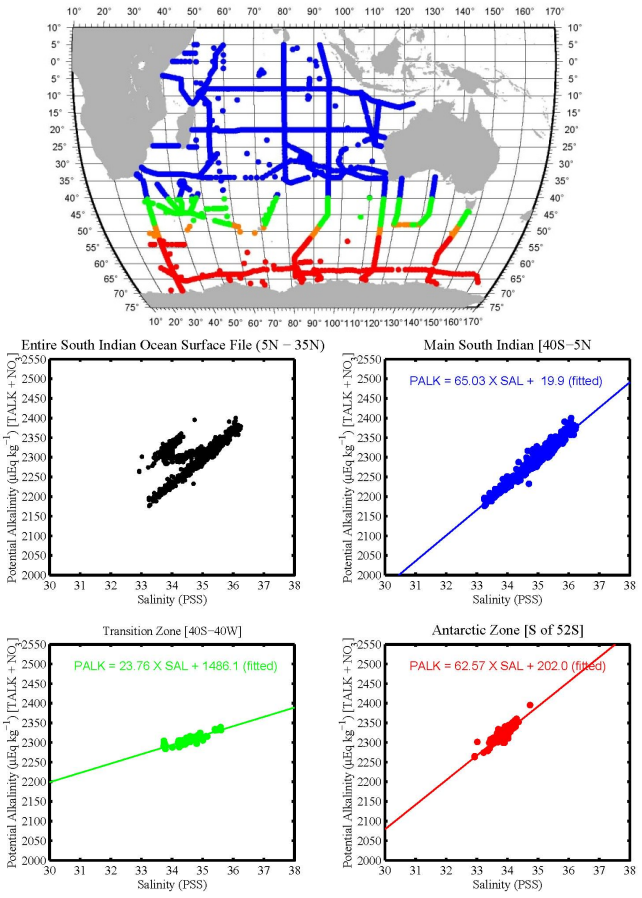

3.2.7 Southern Ocean: (south of 60°S):

The PALK-salinity relationships in each of the Atlantic, Pacific and Indian sectors of the Southern Ocean have been analyzed separately in order to examine the differences between the subtropical waters and the polar waters. As shown in Table 1, the regression slopes and intercept values in each of these sectors vary widely: the regression slopes for the Atlantic and Pacific sectors are 57.8 and 81.7 μeq kg^{-1} per salinity unit respectively. This may be attributed to a narrow salinity range (33.0 - 34.8) as well as to uneven seasonal and spatial distribution of samples. However, in the salinity range of 33.0 to 34.6 in Southern Ocean surface waters, these regression equations give PALK values consistent to each other within a mean difference of ± 8 μeq kg^{-1}. Since the differences between the regression lines for the three sectors are not significantly different in this salinity range, the PALK data in the circumpolar surface waters are grouped together (Figure 9) and represented by a single linear regression line with a RMSD of ± 9.1 μeq kg^{-1} (Table 1): PALK (μeq kg^{-1}) = 74.13 x Salinity (PSS) -192.3). The negative intercept (-192.2 μeq kg^{-1}) may be attributed to greater upwelling of deep waters in higher salinity areas (and more dense waters). This relationship is used for the calculation of the distribution of pH and others, rather than the regression lines for each of the Atlantic, Indian and Pacific sectors. Thus, a total of 24 regions are used in this study for the global ocean analysis.

Figure 9 – Sample locations (left) and the PALK-salinity plot (right) for the Southern Ocean (south of 60°S). The linear regression line and equation are indicated in the data plot and are used to represent the circumpolar Southern Ocean (see text for explanation).

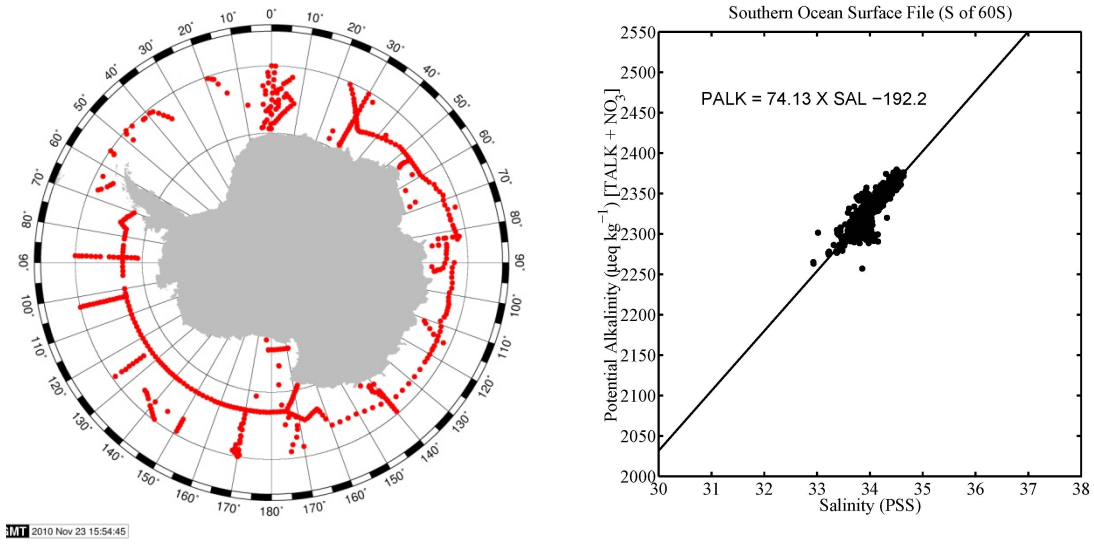

3.3 Global Distribution of Total Alkalinity:

To obtain pH, degree of saturation for $CaCO_3$, the values for TALK and pCO_2 are needed. First, the global distribution of PALK is obtained using its relationship with salinity for the 24 ocean regions (Table 1) and the climatological salinity for the global oceans (Antonov et

al., 2010. http://www.nodc.noaa.gov/OC5/WOA09/woa09data.html). Then, the total alkalinity (TALK) is obtained by subtracting the climatological mean monthly concentration of NO_3^- (Conkright et al., 1994) from PALK. All the values are reassembled to conform to our 4° x 5° grid for each month. The monthly TALK values in 4° x 5° boxes are listed in this report as well as in our LDEO web site: GLOBAL pH MAPS & TALK section in www.ldeo.columbia.edu/CO2.

The global distribution of TALK thus computed is shown in Figure 10 for February and August, and the TALK values for each of 12 months are used with pCO_2 data for the computation of other carbonate chemistry parameters. In the gridded data file as well as in Figures 10, 11, 16, 17, 18 and 19 (for TALK, pH, Ωaragonite, Ωcalcite and TCO_2 respectively), the equatorial Pacific boxes, which are marked with "+" in the figures, are left blank. Because of the large and irregular interannual variability induced by the reorganization of ocean dynamics during the El Niño and La Niña events (Feely et al., 2002), the available TALK and TCO_2 measurements are not enough to compute reliable mean values for each of these phases separately. In contrast to the equatorial Pacific zone, the dynamics of subpolar-subtropical frontal zones (marked "Transition Zone" without regression lines in Table 1) is dominated by eddy mixing and meandering of the front without major reorganization of ocean dynamics. The large variation of the TALK and TCO_2 data are likely to be due primarily to the lateral mixing of the water masses within the transition zone. Accordingly, the mean box values in this zone are approximated by linearly interpolating from the adjacent boxes and marked with dots in the figures.

Figure 10 shows that the subtropical North and South Atlantic Oceans have the highest TALK values among the global oceans due primarily to the high salinity caused by the high E/P ratios, whereas the tropical and subtropical Indian Ocean has lower values. The high values in the Arabian Sea are due primarily to the upwelling of deep waters, and the low values in the Bay of Bengal are caused by the low salinity river waters. The low salinity waters (33.5> Sal >25.5) for the Bering Sea and the Arctic have the lowest TALK values, which are attributable to excess precipitation and ice melting in the region. In contrast to the subarctic and Arctic waters, TALK in the Southern Ocean is similar to the mid-latitude waters. This may be due to higher salinity (34.2> Sal > 33.7) and upwelling of high TALK subsurface waters.

The seasonal variation of TALK is generally small over the tropical and subtropical oceans, reflecting small changes in salinity and NO_3^-. Small changes are also found in the subpolar and polar waters, where large seasonal changes as large as 30 μeq kg^{-1} are anticipated due to seasonal NO_3^- changes associated with biological activities. Contrary to the expectation, the observed seasonal changes (Figure 10) are found to be much smaller within a range of ± 5 μeq kg^{-1} in the subpolar regions of the both hemispheres. This may be accounted for by the near cancelation of the salinity effect with the NO_3^- effect: TALK is decreased by lower salinity in summer (due to increase in E/P), whereas it is increased by lower NO_3^- concentrations in summer (due to biology). For example, in the subarctic western Pacific (54°N-58°N and 162.5°E-157.5°W), TALK is reduced by 18 (± 13) μeq kg^{-1} in summer due to a lowering of summer salinity by 0.3 (± 0.2) PSS, and is increased by 16 (± 2) μeq kg^{-1} by the reduction of NO_3^-, resulting in a net reduction of 2 (± 14) μeq kg^{-1}, which compares with the observed mean reduction of 4 (± 20) μeq kg^{-1}. The salinity effect may exceed the opposing effect of biology or vice versa, and the seasonal amplitude of TALK is not only reduced, but also its sign for the seasonal change of TALK may be reversed depending upon the magnitude of changes in salinity and NO_3^-.

Figure 10 – Climatological mean distribution of the total alkalinity (TALK) over the global ocean with a 4° x 5° resolution. The TALK values are computed using the potential alkalinity-salinity relationships (measured during 1990-2008) (Table 1) and the climatological mean monthly values for surface water salinity (Antonov et al., 2010) and concentrations of nutrients (Conkright et al., 1994). The black dots indicate transition zones between the subtropical and subpolar waters, where the TALK values vary irregularly. The TALK values in these areas are interpolated using adjacent pixel values. The equatorial Pacific areas marked with "+" symbols are excluded from the analysis because of the large interannual changes associated with El Niño events.

A) February

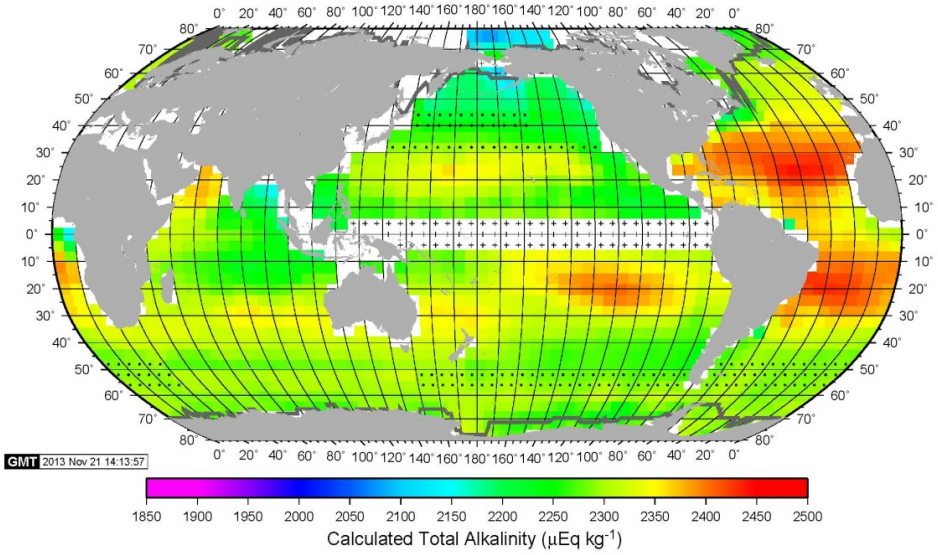

B) August

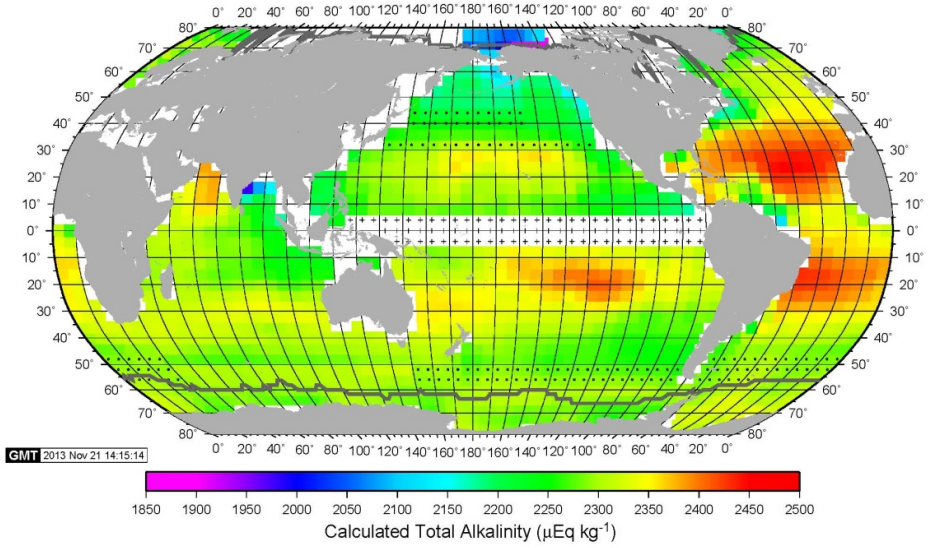

3.3.1 Comparison with Previous Studies:

Two major studies on the distribution of TALK in the global ocean have been published prior to this study. Analyzing 1,700 surface alkalinity data from GEOSECS, TTO, WOCE and other programs, Millero et al. (1998) divided the world ocean into 6 regions and expressed the salinity normalized alkalinity as a quadratic function of temperature. More recently, Lee et al. (2006) divided the oceans into 5 regions, and proposed TALK formulations for each region as a quadratic function of both salinity and temperature. In these studies, water temperature was used as a proxy representing the complex oceanographic processes including changes in the net community production, $CaCO_3$ precipitation and dissolution, and lateral and vertical water mixing. In contrast, we divide the oceans into 24 regions, and consider that the salinity is the primary driver for alkalinity, and nitrate is a secondary driver reflecting the direct effect on alkalinity of seasonal changes in the net primary production.

Figure 11 shows a pair of the maps for February and August indicating the differences between the values obtained with Lee et al. (2006) formulations and this study expressed as [(Lee et al.) – (This work)]. The Lee et al. values are computed using the same salinity and temperature values as those used in our study. In general, the Lee et al. formulations yield TALK values consistent with our estimates on the global average. The tropical and subtropical Atlantic and Indian Oceans are in a close agreement. On the other hand, our values for the subtropical Pacific oceans tend to be greater than the Lee et al. up to 15 $\mu eq\ kg^{-1}$. In their study, they expressed the subtropical Pacific, Atlantic and Indian Oceans (30°N-30°S) with a single formula, whereas, in our study, each of these three oceans is expressed using a number of region specific formula. The differences may be attributed to the Lee et al. method, in which the three oceans are expressed by a single formula.

In the polar and subpolar Southern Oceans, our values differ from Lee et al. seasonally by $\pm$ 15 $\mu eq\ kg^{-1}$. In the subarctic and Arctic regions, the Lee et al. values are lower than ours by as much as 50 $\mu eq\ kg^{-1}$. These differences may be attributed to the inclusion of newer data in our study. In the northwestern subarctic Pacific including the Bering Sea (the red areas in Figure 11), we find that Lee et al. formulation yields much greater TALK values (up to 60 $\mu eq\ kg^{-1}$) than ours. Lee et al. compared their results with those of Millero et al. (1998), and showed (in Figure 4 of Lee et al., 2006) that their values in the subarctic Pacific (north of 30°N; their Zone 4) are greater than Millero et al. (north of 30°N; their Zone 5) by as much as 30 $\mu eq\ kg^{-1}$. Our results are more consistent with those of Millero et al. In the Lee et al. formula for the North Pacific (Zone 4), they added "longitude" (the unit unspecified) as an extra parameter for describing the east-west gradient. This parameterization scheme may have caused excessively high TALK values in this region.

It should be pointed out that, despite the regional and seasonal differences among these three studies, the RMSD values for the respective formulations are similar to each other in a range of $\pm$ 5 to $\pm$ 9 $\mu eq\ kg^{-1}$, which are consistent with the reported precision of measurements. This suggests that, while these studies used different parameters for fitting the data, these methods yield statistically comparable results in representing the overall global observations.

Figure 11- Differences, (Lee et al. – This study) in μeq kg^{-1}, between the surface water alkalinity values by Lee et al. (2006) and this study: A) February, and B) August. The Lee et al. values are computed using the climatological mean temperature and salinity data used in this study. The differences are expressed by. No estimates are given for the equatorial Pacific (marked with the "+" symbols). The heavy grey curves indicate the ice edges.

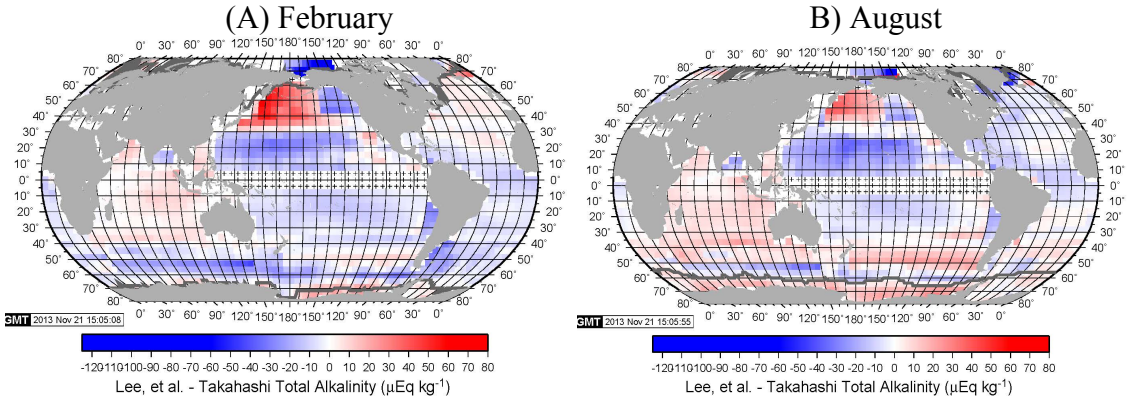

3.4 Climatological Distribution of Surface Water pCO_2:

For the second carbon chemistry parameter needed for computing pH and related properties, we select pCO_2 in surface ocean water. Its climatological monthly mean values over the global ocean are compiled for a 4° x 5° grid for the reference year 2005, and the gridded data for each of 12 months are listed in this report (also available at our web site www.ldeo.columbia.edu/CO2). The February and August values are shown in Figure 12. This is an updated version of Takahashi et al. (2009) for the reference year 2000 representing non-El Niño years using about 2.5 million new data acquired since then. Of about 6.5 million pCO_2 data observed in 1957-2012 (Takahashi et al., 2013), about 0.2 million for the El Niño periods and 0.6 million for the coastal waters (within 1° x 1° from land) were removed, and the remaining 5.7 million data are used to compute a climatology for non-El Niño period using the time-space interpolation method (Takahashi et al., 2009) based on a 2-D diffusion-advection transport equation.

Figure 12 – Climatological mean distribution of the surface water pCO_2 over the global oceans in the reference year 2005: (A) February, and (B) August. These maps have been up-dated to the reference year 2005 using a total of about 5.6 million pCO_2 measurements (Takahashi et al., 2013) which include about 2.5 million new data acquired since 2000. The orange-yellow colors indicate CO_2 source areas for the atmosphere, and the cyan-blue and magenta areas are sink areas for atmospheric CO_2. The heavy pink curves indicate the mean position of the equator-ward extent of ice fields.

A) February, 2005

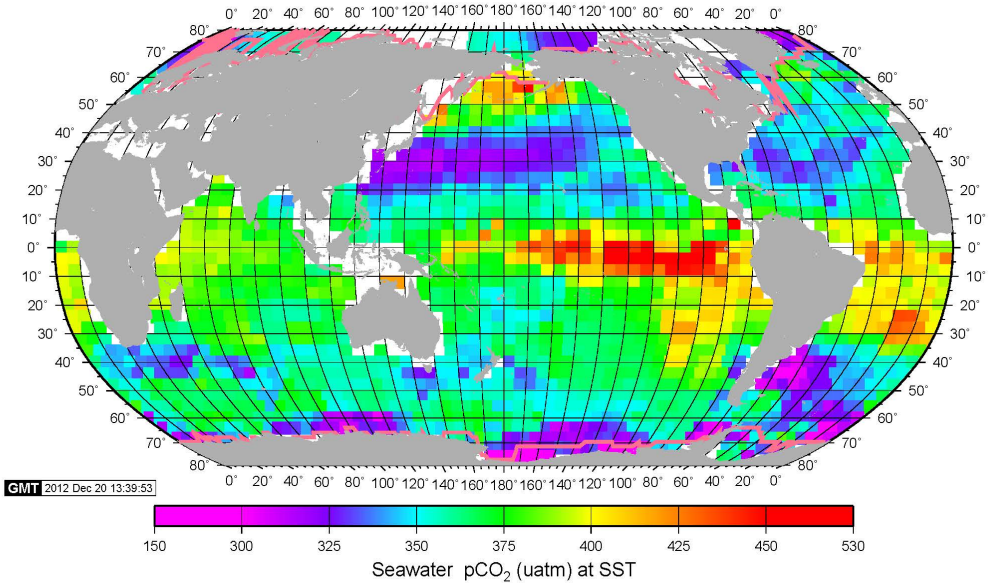

B) August, 2005

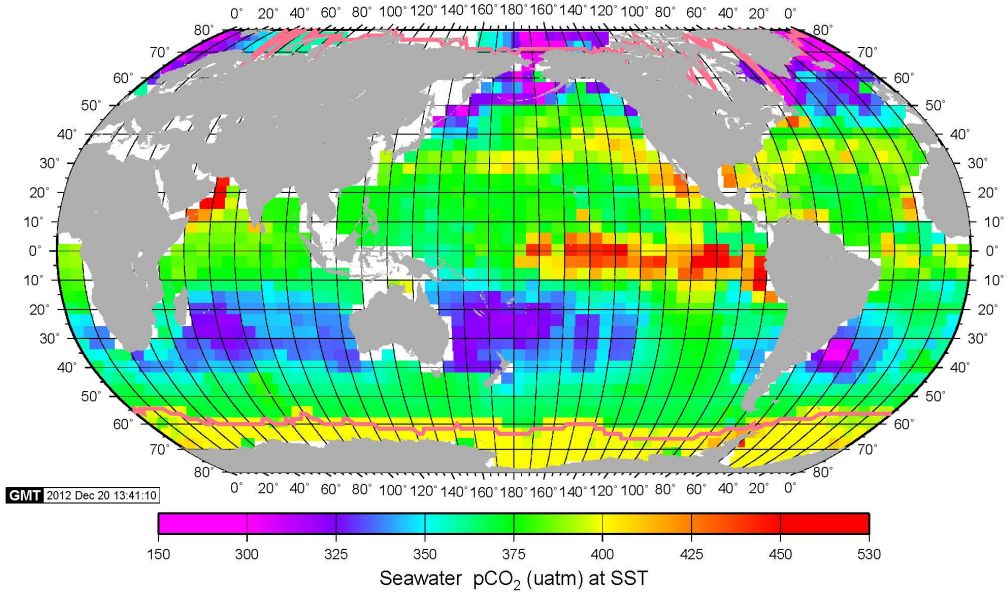

Large seasonal changes observed in the subtropical gyre areas are attributed primarily to the seasonal temperature changes, whereas the changes in the subpolar and polar areas are due to upwelling of deep waters in winter and intense photosynthesis during summer. The differences between the 2005 and 2000 climatologies are shown in Figure 13. The differences, however, are attributable partially to the improved database, and, hence, do not necessarily represent changes occurred in the ocean. Compared to the 2000 climatology by Takahashi et al. (2009), the 2005 pCO_2 values are 10 ± 3 μatm greater on the average.

Figure 13 - Differences, (2005 – 2000) in μatm, in surface water pCO_2 climatologies between the reference years 2000 and 2005: (A) February and (B) August. Note that the changes are attributable not only to changes occurred in the ocean, but also to the 2.5 million new observations added since the 2000 climatology of Takahashi et al. (2009).

(A) 2005-2000 pCO_2 difference (μatm) in February

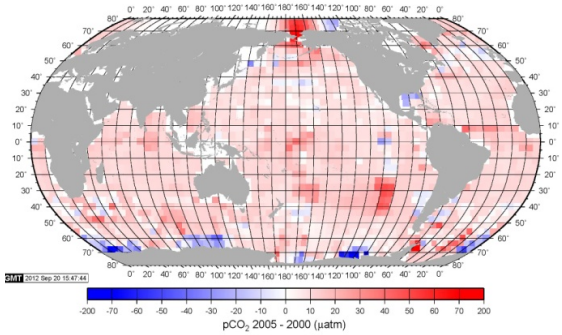

(B) 2005-2000 pCO_2 difference (μatm) in August

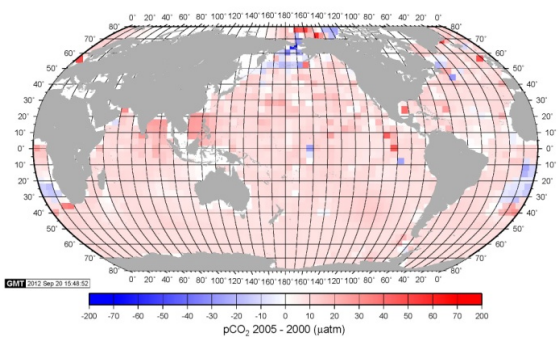

---

4. VALIDATION TESTS FOR THE ESTIMATED VALUES

The validity of our pCO_2-potential alkalinity method is tested by comparing the calculated TCO_2 values with the observed values. We present below a comparison of the monthly values at three well established time-series stations (BATS, HOT and ESTOC) as well as at a number of other areas where some observations are available. Since these time-series data are not included in our "LDEO_SurCarbChem" database, a comparison of the seasonal variation of the measured and computed TCO_2 or pH should provide an independent test for the reliability of the method used in this study.

4.1 Time-series Stations, BATS, HOT and ESTOC:

Detailed tests may be made by comparing the monthly observations made during the Bermuda Atlantic Time Series (BATS) program (Bates et al., 2012), the Hawaii Ocean Time-series (HOT) program (Dore et al., 2009; Fujieki et al., 2012), and the European Time Series in the Canary Islands (ESTOC) program (Santana-Casiano et al., 2007; Gonzalez-Davila and Santana-Casiano, 2009). Figure 14 shows that the computed TCO_2 values for 2005 from the estimated TALK and pCO_2 values (open red circles) for the BATS and HOT sites reproduce closely the observed values in 2005-2006 (filled black circles). For the ESTOC site, the calculated pH values at 25 °C from the pCO_2 and alkalinity are compared with the measured values at 25 °C. Although the computed pH values are higher than the observed by about 0.01 during the later summer months, they are consistent with the observations for the rest of the year. This gives further credence to the pH values obtained by the pCO_2-TALK method used in this study.

Figure 14 – Comparison of the observed and calculated values at the three time-series stations: A) TCO_2 at the BATS station in the western North Atlantic, B) TCO_2 at the HOT station in the North Pacific, and C) pH (25°C) at the ESTOC station in the eastern North Atlantic. The 2005-2006 observations are shown with filled black circles, and the calculated values for 2005 in the

4° x 5° boxes which include these stations are shown with open red circles. The BATS station is located in the 4° x 5° box centered at 32°N and 62.5°W, and the ESTOC station in the box centered at 28°N and 17.5°W. The HOT station is located north of Hawaii near the border of two 4° x 5° boxes, and the computed values for the box centered at 20°N and 157.5°W are shown. The computed TCO_2 values are consistent with the observed, capturing the seasonal variability.

(A) BATS (31.7°N, 64.2°W) (B) HOT (22.7°N, 158°W)

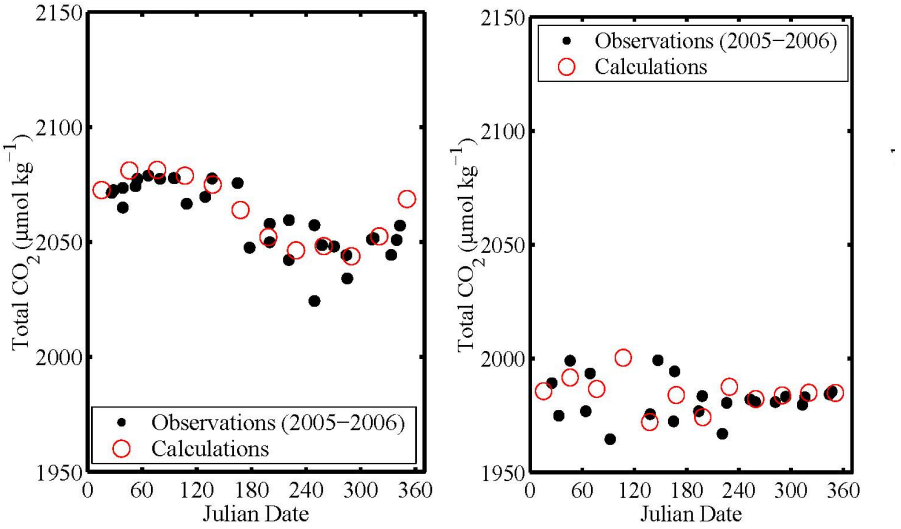

(C) ESTOC (29.1°N, 15.8°W)

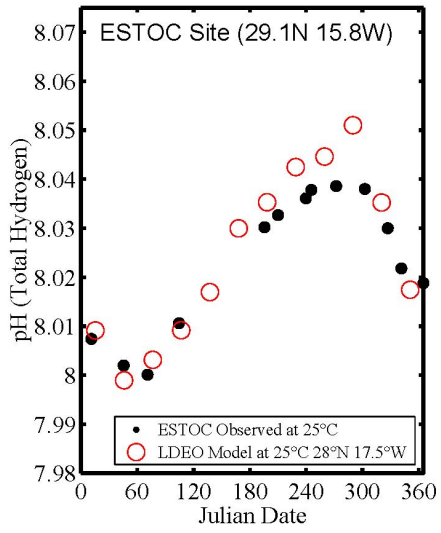

4.2 Other Ocean Areas:

The computed TCO_2 values are compared with the observations in 18 areas located in various ocean regimes. Figure 15 shows a comparison of the observed TCO_2 data (filled black circles) with those computed (red open circles) from the 2005 pCO_2 and potential alkalinity-

salinity relationships in various oceanographic regimes including the Iceland Sea, Drake Passage, North Atlantic, North Pacific and Indian Oceans. Although the TCO_2 values were measured in different years and it has increased at a mean rate of less than 1 μmol kg^{-1} yr^{-1} by the uptake of atmospheric CO_2, no adjustment is made for the difference between the reference year and year of observation. With the exception of a few ocean areas where different water types meet and mix, the observed TCO_2 values are consistent with those calculated from and pCO_2, and PALK. In the northwestern Pacific east of the Kamchatka peninsula (top row, second from right in Figure 15-D), the observed values near the day 240 (late August) exceed the computed values by as much as 100 μmol kg^{-1}. In this box area, the Oyashio Current is joined by a narrow low-salinity water flowing out from the Bering Sea. In the northeastern Indian Ocean (Figure 15-E), the large deviations seen in the late summer may be attributed to the influx of the Indus river in the Arabian Sea and the Ganges-Brahmaputra river waters in the Bay of Bengal. These deviations are attributed to erroneous TALK values that result from the failure of the PALK-salinity relationships to include the influx of different water types. These small scale structures cannot be adequately represented by the 4° x 5° spatial resolution used in this study, indicating the limitation of this study.

Figure 15 – Comparison of the observed TCO_2 with the climatological mean seasonal variability of TCO_2 in the reference year 2005 in 4° x 5° box areas in (A) the northern (near Iceland) and southern (Drake Passage) subpolar oceans, (B) the North Atlantic, (C) the western subarctic northeast and central Pacific Ocean, (D) the subarctic northwest Pacific and (E) the northern Indian Ocean. The open red circles indicate the calculated values for 2005, and the filled black circles indicate the observed values without adjustments for changes due to atmospheric CO_2 uptake. The center position of each 4° x 5° box is indicated at the top of each panel. The most of the computed TCO_2 values are consistent with the measured values. The exceptionally large deviations are found in the northwestern Pacific and northern Indian Oceans, where waters of different properties meet and mix.

A) Sub-polar Oceans

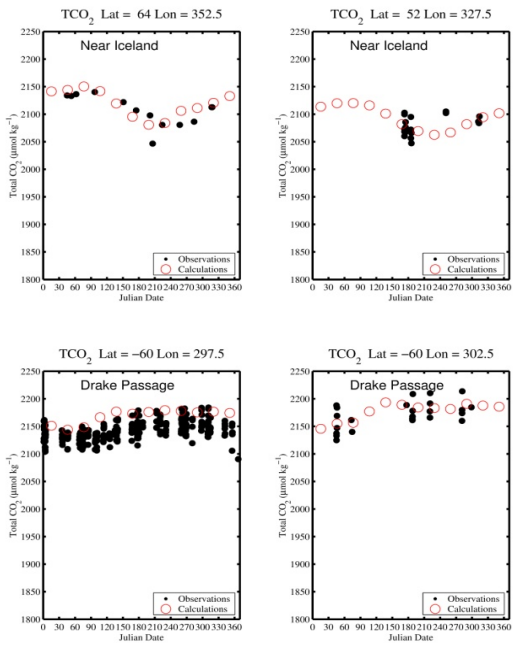

B) North Atlantic

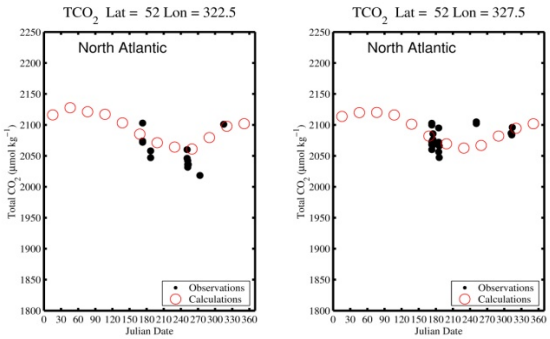

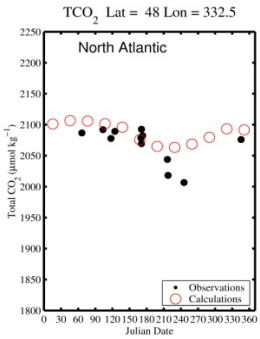

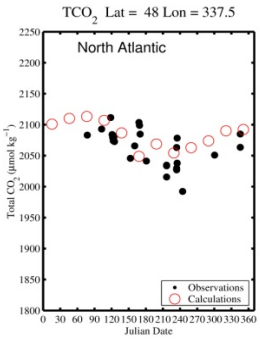

C) Sub-arctic Northeast and central Pacific

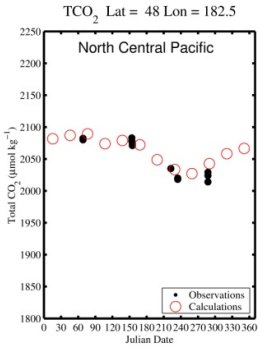

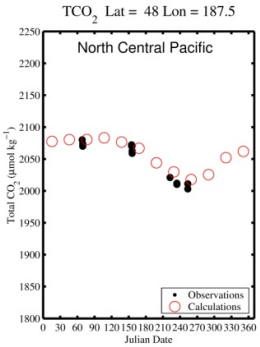

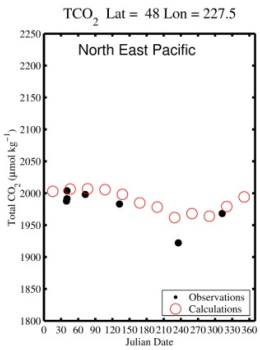

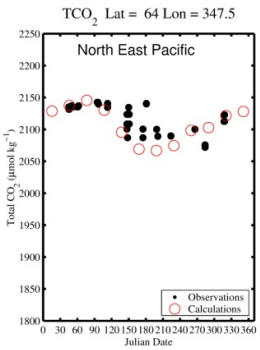

D) Sub-arctic Northwest Pacific

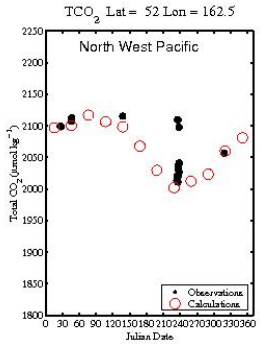

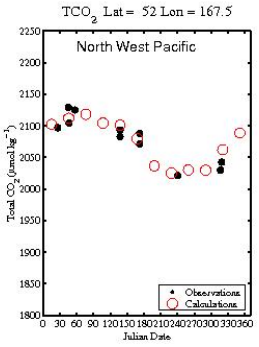

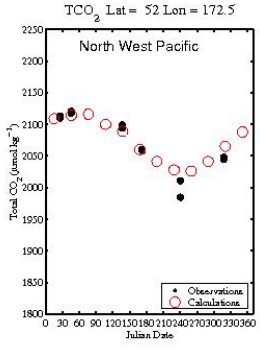

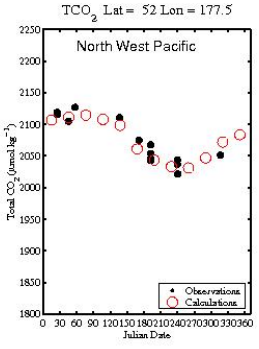

E) North Indian Ocean:

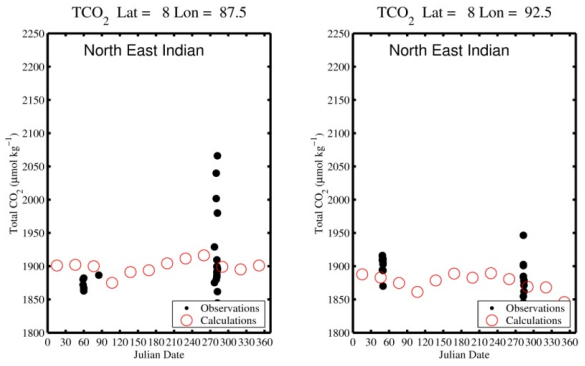

---

5. CLIMATOLOGICAL MEAN DISTRIBUTION

The climatological mean distribution maps for pH, degree of saturation for aragonite and calcite in surface waters of the global oceans for the reference year 2005 are presented in this section. These are calculated using the following climatologies; a) climatological mean monthly pCO_2 in surface water in 4° x 5° box areas for the reference year 2005 (see Section 3.4); b) the potential alkalinity-salinity relationships representing 24 oceanic areas (based on the measurements made 1990-2008, Section 3.2); c) climatological mean monthly values for surface water temperature (NCEP Reanalysis data, 2001), salinity (Antonov et al., 2009) and concentrations of nutrients (Conkright et al., 1994)); and d) the inorganic carbonate chemistry model (Section 2). The degree of saturation for aragonite and calcite is expressed in $\Omega = [Ca^{++}]_{sw} \times [CO_3^{=}]_{sw} / Ksp'$, where Ksp' is the solubility products $CaCO_3$ formulated by Mucci (1983) for aragonite and calcite. The calcium concentration in seawater is approximated by $[Ca^{++}]_{sw}$ (mol kg^{-1}) = 0.01012 x (Salinity)/35. $CaCO_3$ supersaturation is indicated by $\Omega > 1.0$, and undersaturation by $\Omega < 1.0$. The 4° x 5° gridded data for each of 12 months are shown in this report (also available at our web site, www.ldeo.columbia.edu/CO2).

On the basis of the estimated uncertainties for TALK and pCO_2 of ± 10 μeq kg^{-1} and ± 10 μatm respectively, the combined uncertainty for each of the computed properties is estimated to be ± 0.01 for pH, ± 0.06 for Ωaragonite, ± 0.09 for Ωcalcite, and ± 10 μmol kg^{-1} for TCO_2.

5.1 pH:

The pH values presented in this paper are in the total H^+ ion scale, which is the concentration of free H^+ plus HSO_4^- ions (Dickson, 1993), and the distribution at in situ surface water temperature is presented in Figure 16 for February and August. The values for these and the other months are listed in our web site. The pH values range from 7.9 to 8.2 in 2005. Lower (more acidic) values are found in the upwelling regions in the Panama Basin (in the equatorial Pacific), Arabian and Bering Seas; and higher values are

found in the subpolar and polar waters during the spring-summer months of intense photosynthetic production. The vast areas of subtropical oceans have seasonally varying pH values ranging from 8.05 during warmer months to 8.15 during colder months: 25% change in the H^+ ion concentration. In contrast, pH in the high-nutrient subpolar and polar waters is lower during winter due to the upwelling of more acidic deep waters, and increases during summer due to intense photosynthetic utilization of CO_2. Accordingly, the seasonal pH change in subpolar oceans is about six months out of phase from that in the adjacent subtropical ocean.

Figure 16 –The climatological mean distribution of pH (total H^+ ion scale at in situ temperatures) in the global ocean surface water in (A) February and (B) August in the reference year 2005. The pink curves indicate the positions of the mean equator-ward front of seasonal ice fields. The "+" symbol indicates the box areas affected by the El Niño events, and no value is given. The boxes with black dots are in transition zone between oceanographic regimes (such as subtropical to subpolar regimes), where the pH values are highly variable. The values in these boxes are interpolated from the adjacent box values.

(A) Calculated pH for February, 2005

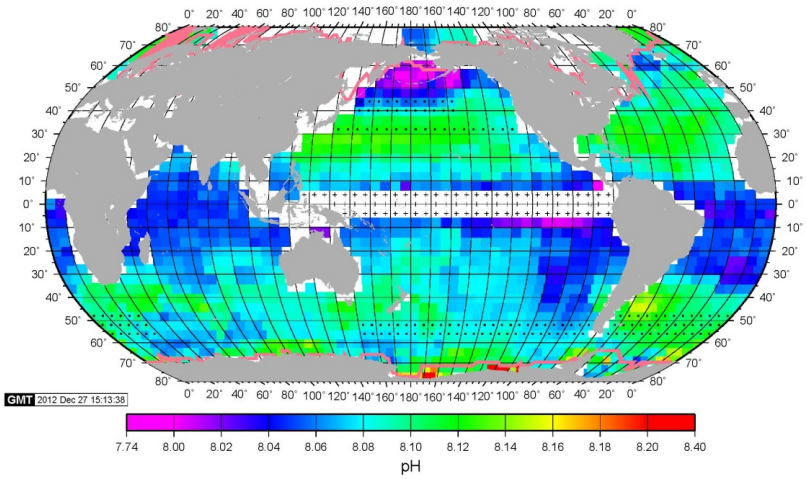

(B) Calculated pH for August, 2005

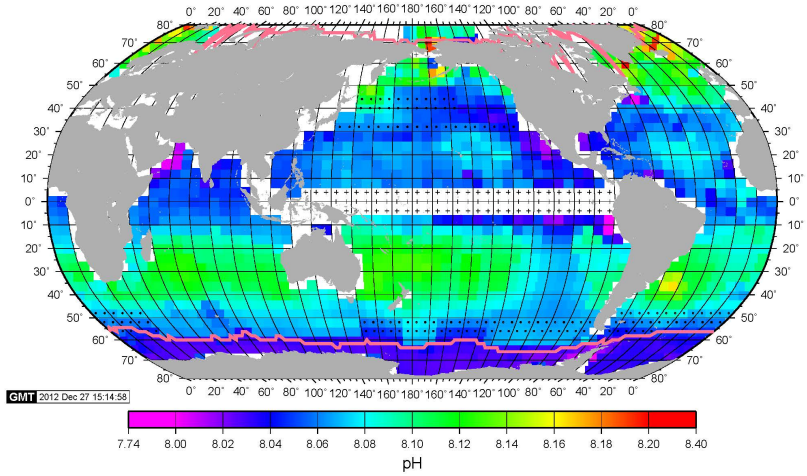

5.2 Degree of Saturation for Aragonite and Calcite:

Surface waters of the global oceans are generally supersaturated with respect to aragonite and calcite. As shown in Figure 17, the warm tropical and subtropical waters are supersaturated with respect to aragonite by a factor of about 4, whereas the cold subpolar and polar waters are supersaturated only by 1.2 (or 20% supersaturation) or less. However, the western Arctic waters become undersaturated in summer with Ωaragonite ranging from 0.9 in summer months to 1.2 in winter months. In recent studies in the western and central Arctic, aragonite undersaturation (Ω as low as 0.8) has been reported (Bates and Mathis, 2009; Bates et al., 2009; Chierici and Fransson, 2009; Robbins et al., 2013). On the other hand, the Southern Ocean waters in the seasonal ice zone are supersaturated with aragonite by 1.3 to 1.5 throughout a year.

Figure 17 shows that, while the aragonite Ω values for the subtropical Pacific and Atlantic are similar, those in the subtropical Indian Ocean are generally lower (i. e. less saturated, more yellowish in the maps). This reflects the lower pH values (Figure 16), and the possible causes for the uniqueness of the Indian Ocean will be discussed later in the Section 5.4.

Figure 17 –The climatological mean distribution of aragonite saturation level (Ω) in the global ocean surface water in (A) February and (B) August in the reference year 2005. The pink curves indicate the positions of the mean equator-ward front of seasonal ice fields. The "+" symbol indicates the box areas affected by the El Niño events, and no value is given. The boxes with black dots are in transition zone between oceanographic regimes (such as subtropical to subpolar regimes), where the Ω values are highly variable. These values are interpolated from the adjacent box values. Note that the Arctic Ocean is slightly undersaturated ($\Omega \leq 1.0$), whereas the seasonal ice zone in the Southern Ocean is 10% to 20% above the saturation.

A) February, 2005

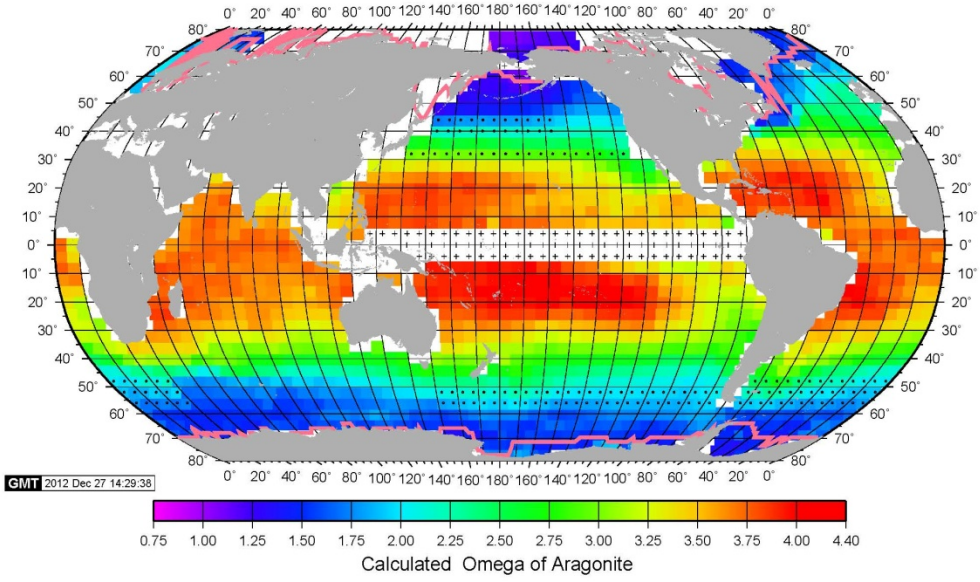

B) August, 2005

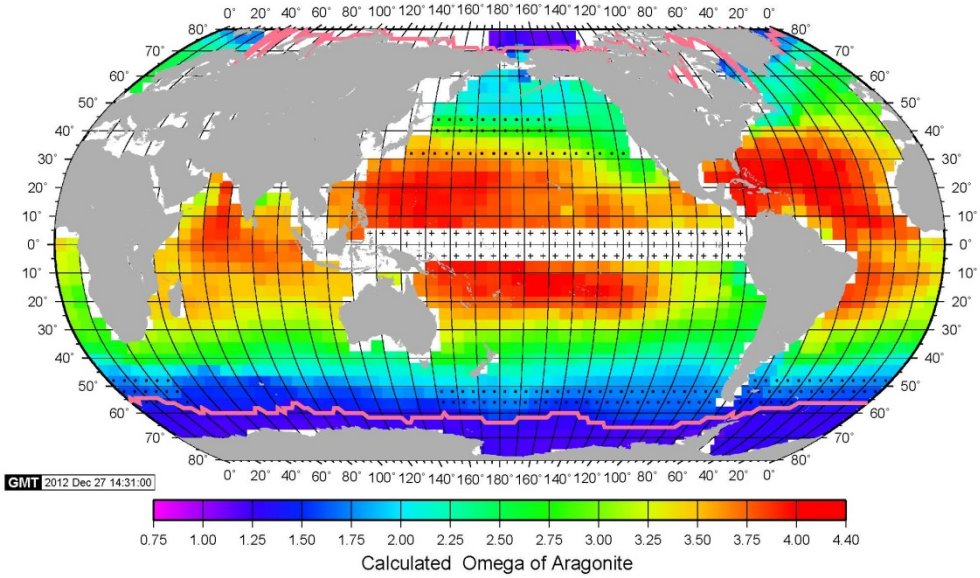

The distribution maps of calcite saturation for February and August, 2005, are shown in Figure 18. The Ω values range between 1.7 in the polar regions to 6.3 in subtropical waters. In the Southern Ocean, the Ω values for calcite are as low as 1.7 in the under-ice waters due to the upward mixing of high CO_2 deep waters, and it is about 2.3 in the seasonal ice zone waters. The global pattern of distribution is similar to that for aragonite, and the north and south Indian Oceans are shown to have lower degree of saturation than the Pacific and Atlantic, as will be discussed in Section 5.4.

Figure 18 – The climatological mean distribution of calcite saturation level (Ω) in the global ocean surface water in (A) February and (B) August in the reference year 2005. The pink curves indicate the positions of the mean equator-ward front of seasonal ice fields. The "+" symbol indicates the box areas affected by the El Niño events, and no value is given. The boxes with black dots are in a transition zone between oceanographic regimes, where Ω values are highly variable. These values are interpolated using the adjacent box values.

A) February, 2005

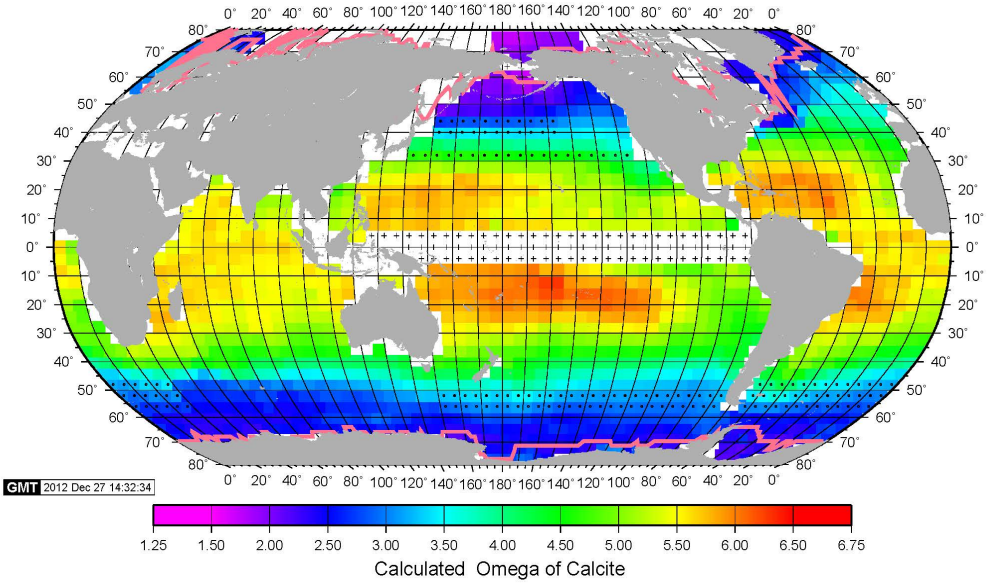

B) August, 2005

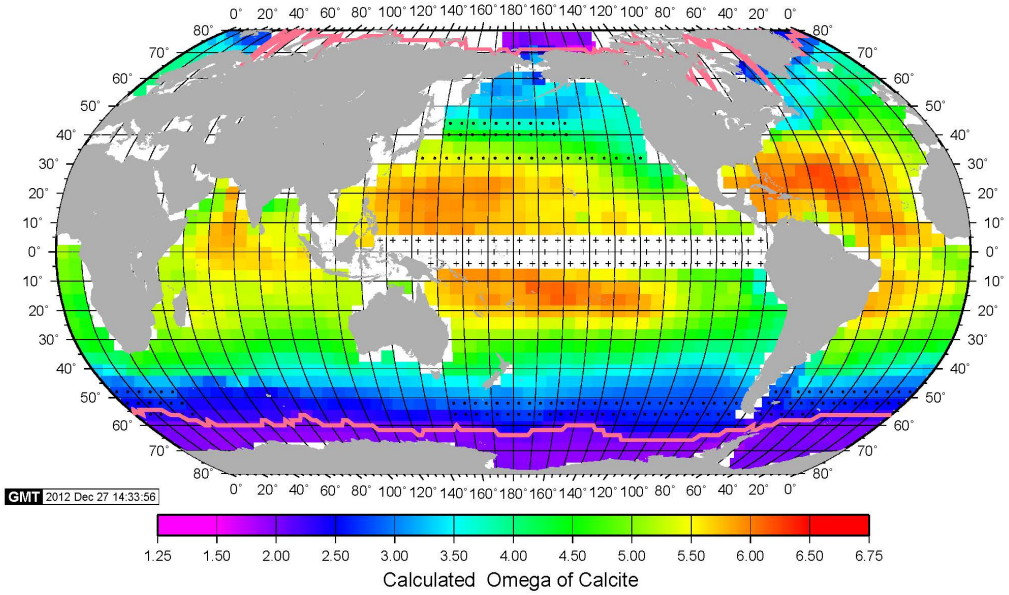

5.3 TCO_2 in surface water:

The distribution maps of TCO_2 calculated for February and August, 2005, are shown in Figure 19. The TCO_2 values range between 2,225 μmol kg^{-1} in polar regions to 1,875 μmol kg^{-1} in subtropical waters. They are higher during winter reflecting greater upward mixing of high-CO_2 deep waters, and are lower during summer due to the biological CO_2 utilization. The amplitude for seasonal change is generally about 75 μmol kg^{-1} for the subpolar waters, while that for subtropical waters is smaller and correlates with the seasonal SST amplitude. The TCO_2 in under-ice waters in the Southern Ocean is as high as 2,230 μmol kg^{-1} (Figure 19-B) because of the upwelling of deep waters and the reduced sea-air CO_2 gas exchange by ice cover.

The north and south Indian Oceans are shown to have lower TCO_2 values than the Pacific and Atlantic. The causes for this feature will be discussed below.

Figure 19 –The climatological mean distribution of TCO_2 in the global ocean surface water in (A) February and (B) August in the reference year 2005. The TCO_2 values are computed using the total alkalinity (TALK) and pCO_2. The pink curves indicate the positions of the mean equator-ward front of seasonal ice fields. The "+" symbol indicates the box areas affected by the El Niño events, and no value is given because of large space-time variability. The boxes with black dots are in transition zone between oceanographic regimes (such as subtropical to subpolar regimes), where TCO_2 values are highly variable. These values are interpolated using the adjacent box values.

A) February, 2005

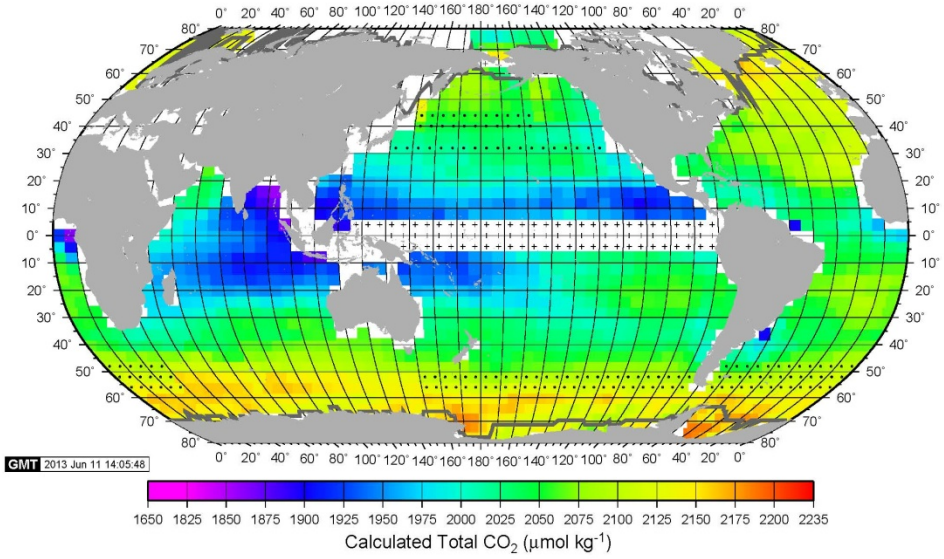

B) August, 2005

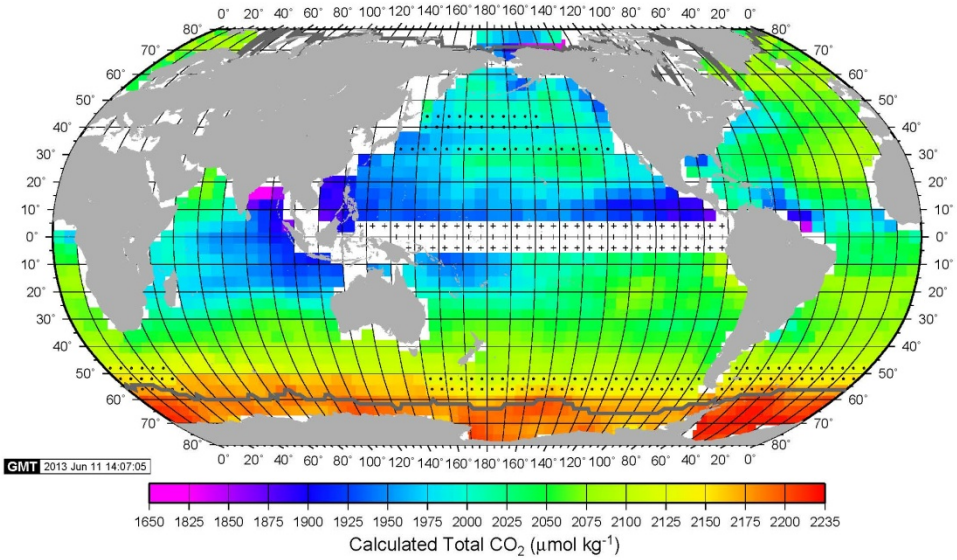

5.4 Regional Variability:

Figure 16 shows that the northern Indian Ocean has lower pH than the subtropical North Pacific and North Atlantic in the corresponding latitudes, especially during the northern winter months. All other carbon chemistry properties north of about 30°S are different from the Pacific and Atlantic Oceans. In the Indian Ocean, TALK is lower (Figure 10) and pCO_2 is higher (Figure 12) than the Atlantic and Pacific. The computed properties including pH (Figure 16), Ω for aragonite and calcite (Figures 17 and 18) and TCO_2 (Figure 19) are all lower in the Indian Ocean than the Atlantic and Pacific reflecting these differences. The causes for these differences are not understood because of the complexity which is unique to the Indian Ocean. In the northwestern Indian Ocean, the Arabian Sea receives a number of different waters including a) the intense summer upwelling of deep waters, b) high salinity warm outflow waters from the Red Sea and Persian Gulf, and c) the Indus River waters. The northeastern Indian Ocean and the Bay of Bengal receive from the east the low salinity Indonesian outflow and from the north the Ganges- Brahmaputra River waters. The proportions of these waters vary seasonally as well as annually. The Arabian Sea water is generally warmer and saltier than the Bay of Bengal. Furthermore, the surface water circulation is reorganized extensively in response to the monsoons. Biological differences, which reflect these physical and chemical differences, may play a role in regulating the carbon chemistry in the Indian Ocean waters. Therefore, further observational and model studies are needed for improved understanding of the uniqueness of the Indian Ocean.

Significant differences between the subarctic Pacific and Atlantic are shown for the alkalinity (Fig. 10), pH (Fig. 16), the $CaCO_3$ saturation (Figs.17 and 18) and TCO_2 (Fig. 19). The role of the large scale ocean circulation on biogeochemical contrasts between the Pacific and Atlantic has been presented extensively in ocean circulation model studies (e. g. Gruber et al., 2009). In the Atlantic, the warm saline Atlantic surface water with high alkalinity flows northward into the GIN Seas and the Arctic basin. In the Pacific, the northward transport of the less saline open Pacific water into the

Bering Sea is impeded partially by the Aleutian Arc, and the flow of the Bering Sea water into the Arctic basin is slow ranging between 0.7 Sv and 1 Sv (Woodgate et al., 2006) due to the shallow Bering Strait. Very large seasonal changes observed in the Bering Sea may be attributed to the long residence time of waters over the broad shallow shelf areas, where pH and $CaCO_3$ saturation level are lowered by vertical mixing of subsurface waters during winter and are increased by intense photosynthesis in summer (Walsh et al., 1989; Cross et al., 2012; Cross et al., 2013).

6. SUMMARY AND CONCLUSION

1) A database for the alkalinity (TALK), pCO_2 and the concentrations of total CO_2 (TCO_2) and nutrients in the surface ocean waters (depths $\leq$ 50 meters) over the global oceans is assembled by building upon the data synthesis of the GLODAP database (Key et al., 2004) supplemented with the TCO_2-TALK pairs from the CARINA program (Tanhua et al., 2009; Key et al., 2010) and pCO_2 and TCO_2 data from the LDEO database. Coastal water data are not included in the assembled database.

2) The global distribution of surface water TALK is obtained using the linear relationships between potential alkalinity (PALK = TALK + NO_3^-) and salinity in 24 ocean regions. Because of the significant interannual variation associated with El Niño events, the equatorial Pacific zone (4°N - 4°S) is not included in the analysis.

3) The seasonal change in TALK is found to be small even in nutrient-rich subpolar waters where the NO_3^- concentrations vary seasonally over a wide range due to the net community production. This is attributed to partial cancellation of the effects of seasonal changes in salinity and NO_3^-. While TALK is reduced in summer due to lower salinity, it is increased by the reduction of NO_3^- by increased biological utilization.

4) The mutual consistency between TALK-TCO_2-pCO_2 values used for the computation of the pH and the degree of saturation of $CaCO_3$ is tested and validated successfully using the available observations including the time-series data at the BATS, ESTOC and HOT programs.

5) Using the mean monthly pCO_2 data adjusted to a reference year 2005 and the estimated alkalinity, the climatological mean distributions of pH and the $CaCO_3$ saturation levels in global surface ocean waters (not including the coastal domain) are computed for each month of the year 2005.

6) The calculated pH (the total H^+ scale) in the global open-ocean surface waters ranges from 7.9 to 8.2 in the year 2005. Lower values are located in the upwelling regions in the tropical Pacific and in the Arabian and Bering Seas; and higher values are found in the subpolar and polar waters during the spring-summer months of intense photosynthetic production. The vast areas of subtropical oceans (excluding the Pacific equatorial zone and coastal zone) have seasonally varying pH values ranging from 8.05 during warmer months to 8.15 during colder months. The warm tropical and subtropical waters are supersaturated by a factor of as much as 4.2 with respect to aragonite and 6.3 for calcite, whereas the cold subpolar and polar waters are less supersaturated only by a factor of 1.2

for aragonite and 2 for calcite because of the lower pH values resulting from greater TCO_2 concentration and lower $TALK/TCO_2$ ratio. Low salinity waters in the western Arctic Ocean are undersaturated with respect to aragonite.

7) Surface waters of the North Indian Ocean are found to have lower pH (more acid) and higher pCO_2 compared to the corresponding latitudes in the North Pacific and Atlantic Oceans. The cause for this difference is not understood.

7. ACKNOWLEDMENTS

This work is supported by the US National Science Foundation Grant OCE 10-38891. The surface water pCO_2 data over the global oceans were produced with the continued support from the US NOAA Climate Program Office; the Southern Ocean measurements were conducted aboard the RVIB Laurence M. Gould with support from the US National Science Foundation; and a grant from the Comer Science and Education Foundation.

8. REFERENCES CITED

Anderson, L. G., Jutterstrom, S., Kaltin, S., Jones, P. E. and Bjork, G., 2004. Variability in river runoff distribution in the Eurasian Basin of the Arctic Ocean. Journ. Geophys. Res., 109, CO1016, doic:10.1029/2003JC001773, 2004.

Antonov, J. I., D. Seidov, T. P. Boyer, R. A. Locarnini, A. V. Mishonov, H. E. Garcia, O. K. Baranova, M. M. Zweng, and D. R. Johnson, 2010. World Ocean Atlas 2009, Volume 2: Salinity. S. Levitus, Ed. NOAA Atlas NESDIS 69, U.S. Government Printing Office, Washington, D.C., 184 pp. http://www.nodc.noaa.gov/OC5/WOA09/woa09data.html

Balch, W. M., Gordon, H. R., Bowler, B. C., Drapeau, D. T. and Booth, E. S., 2005. Calcium carbonate budgets in the surface global ocean based on MODIS data, J. Geophys. Res., 110, C07001, doi:10.1029/2004JC002560.

Bates, N. R., Michaels, A. F., and Knap, A. H., 1996. Seasonal and interannual variability of oceanic carbon dioxide species at the US JGOFS Bermuda Atlantic Time-series Study (BATS) site, Deep-Sea Res. II, 43, 347–383, doi:10.1016/0967-0645(95)00093-3,Corrigendum: 43, 1435–1435, 1996.

Bates, N. R., 2001. Interannual variability of oceanic CO_2 and biogeochemical properties in the Western North Atlantic subtropical gyre. Deep-Sea Research II, 48(8-9), 1507-1528.

Bates, N. R., 2007. Interannual variability of the oceanic CO_2 sink on the subtropical gyre of the North Atlantic Ocean over the last 2 decades. Jour. Geophys. Res., 112, doi: 10.1029/2006JC003759, 2007.

Bates, N. R. and Mathis, J. T., 2009. The Arctic Ocean marine carbon cycle: evaluation of air-sea CO_2 exchanges, ocean acidification impacts and potential feedbacks. Biogeosciences, 6, 2433-2459. www.biogeosciences.net/6/2433/2009/.

Bates, N. R., Mathis, J. T. and Cooper, L. W., 2009. Ocean acidification and biologically induced seasonality of carbonate mineral saturation states in the western Arctic Ocean. Jour. Geophys. Res., 114, C11007. doi:10.1029/2008JC004862,2009.

Bates, N. R., Best, M. H. P., Neely, K., Garley, R., Dickson, A. G. and Johnson, R. J., 2012. Detecting anthropogenic carbon dioxide uptake and ocean acidification in the North Atlantic Ocean. Biogeosciences, 9, 2509–2522, www.biogeosciences.net/9/2509/2012/doi:10.5194/bg-9-2509-2012.

Brewer, P. G. and Goldman, J. C., 1976. Alkalinity changes generated by phytoplankton growth. Lim. and Oceanogr., 21, 108-117.

Chierici, N., and Fransson, A., 2009. Calcium carbonate saturation in the surface water of the Arctic Ocean: undersaturation in freshwater influenced shelves. Biogeosci. Discuss. 6, 4963-4991.

Conkright, M., Levitus, S. and Boyer, T., 1994. World Ocean Atlas, 1994: Volume 1, Nutrients. NOAA Atlas NESDIS 1, National Oceanic and Atmospheric Administration, Washington, D. C., 150 pp.

Cross, J. N., Mathis, J. T. and Bates, N., 2012. Hydrographic controls of net community production and total organic carbon distributions in the eastern Bering Sea. Deep-Sea Res., II, 65-70, 98-109.

Cross, ,J. N., Mathis, J. T., Bates, N. R., and Byrne, R. H., 2013. Conservative and non-conservative variations of total alkalinity on the southeastern Bering Sea shelf. Marine Chem., 154, 100-112.

Dickson, A. G. and Riley, J. P., 1979-a. The estimation of acid dissociation constants in seawater media from potentiometric titrations with strong base. I. The ionic product of water (Kw). Marine Chem., 7, 89-99.

Dickson, A. G. and Riley, J. P., 1979-b. The estimation of acid dissociation constants in seawater media from potentiometric titrations with strong base. II. The dissociation of phosphoric acid. Marine Chem., 7, 101-109.

Dickson, A. G., 1990. Thermodynamics of the dissociation of boric acid in synthetic seawater from 273.15 to 318.15K. Deep-Sea Res., 37, 755-766.

Dickson, A. G., 1993. pH buffers for sea water media based on the total hydrogen ion concentration scale. Deep-Sea Res., 40, 107-118.

Dickson, A. G., 2001. Reference materials for oceanic CO_2 measurements. Oceanography, 14, 21-22.

Doney, S. C, Fabry, V. J, Feely, R. A., and Kleypas, J. A., 2009. Ocean acidification: the other CO_2 problem. Ann. Rev. Mar. Sci., 1, 169-192

Dore, J. E., Lukas, R., Sadler, D. W. and Karl, D. M., 2003. Climate-driven changes to the atmospheric CO_2 sink in the subtrotical North Pacific Ocean. Nature, 424, 754-757.

Dore, J. E., Lukas, R., Sadler, D. W., Church, M. J. and Karl, D. M., 2009. Physical and biogeochemical modulation of ocean acidification in the central North Pacific. PNAS, 106, 12235-12240. doi:10.1073.pnas.0906044106.

Feely, R. A., Boutin, J., Cosca, C. E., Dandonneau, Y., Etcheto, J., Inoue, H., Ishii, M., LeQuere, C., Mackey, D. J., McPhaden, M., Metzl, N., Poisson, A. and Wanninkhof, R., 2002. Seasonal and interannual variability of CO_2 in the equatorial Pacific. Deep-Sea Res., II, 49, 2443-2469.

Feely, R.A., Doney, S. C. and Cooley, S. R., 2009. Ocean acidification: Present conditions and future changes in high-CO_2 world. Oceanography, 22, 36-47.

Feely, R. A., Sabine, C. L., Byrne, R. H., Millero, F. J., Dickson, A. G., Wanninkhof, R., Murata, A., Miller, L. A. and Greeley, D., 2012. Decadal changes in the aragonite and calcite saturation state of the Pacific Ocean. Glob. Biogeochem. Cycles, 26, GB3001, doi:10.1029/2011GB004157, 2012

Feely, R. A., Wanninkhof, R., Sabine, C. L., Mathis, J. T., Takahashi, T., Khatiwala and Park, G.-H., 2013. Global carbon cycle. In State of the Climate in 2012, Special Supplement to the Bull. Am. Meteorological Soc., 94, No. 8, S72-S75.

Fujieki, L. A., Santiago-Mandujano, F., Fumar, C., Lukas, R. and Church, M., 2012. Hawaii Ocean Time-series, Data Report 21: 2009, November 2012. University of Hawaii, School of Ocean and Earth Science and Technology, 1000 Pope Road, Honolulu, Hawaii 96822, pp. 172. <hahana.soest.hawaii.edu/hot/hot-dogs/bextraction.html>

Gonzalez-Davila, M. and Santana-Casiano, J. M., 2003. Seasonal and interannual variability of sea-surface carbon dioxide species at the European Station for Time Series in the Ocean at the Canary Islands (ESTOC) between 1996-2000. Glob. Biogeochem. Cycles, 17, 1076, doi: 10.1029/2002GB001993, 2003.

González-Dávila, M., Santana-Casiano, J. M. and González-Dávila, E. F., 2007. Interannual variability of the upper ocean carbon cycle in the northeast Atlantic Ocean. *Geophys. Res. Lett.*, **34**, L07608, doi:10.1029/2006GL028145.

Gonzalez-Davila, M., and Santana-Casiano, J. M., 2009. Sea Surface and atmospheric fCO_2 data measured during the ESTOC Time Series cruises from 1995-2009. http://cdiac.ornl.gov/ftp/oceans/ESTOC_data/. Carbon Dioxide Information Analysis Center, Oak Ridge National Laboratory, US Department of Energy, Oak Ridge, Tennessee. doi: 10.3334/CDIAC/otg.TSM_ESTOC

González-Dávila, M., Santana-Casiano, J.M., Rueda, M.J. and Llinás, O., 2010. The water column distribution of carbonate system variables at the ESTOC site from 1995 to 2004. *Biogeosciences*, **7**, 3067–3081, doi:10.5194/bg-7-3067-2010.

Gruber, N., Gloor, M., Mikaloff Fletcher, S. E., Doney, S. C., Dutkiewicz, S., Follows, M., Gerber, M., Jacobson, A. R., Joos, F., Lindsay, K., Menemenlis, D., Mouchet, A., Műller, S. A., Sarmiento, J. L. and Takahashi, T., 2009. Oceanic sources, sinks, and transport of atmospheric CO_2. Glob. Biogeochem. Cycles., 23, GB1005, doi:10.1029/2008GB003349,2009.

Gruber, N., Hauri, C., Lachkar, Z., Loher, D., Frölicher, T. and Plattner, G-K, 2012. Rapid progression of ocean acidification in the California Current System, Science, 337, 220-223.

Hales, B. and Takahashi, T., 2004. High-resolution biogeochemical investigation of the Ross Sea, Antarctica, during the AESOPS (U. S.JGOFS) Program . Global Biogeochem. Cycles, Vol. 18, No. 3, GB3006, doi. 10.1029/2003GB002165

Hauri, C., Gruber, N., Vogt, M., Doney, S. C., Feely, R. A., Lachkar, Z., Leinweber, A., McDonnell, A. M. P., Munnich, M. and Plattner, G.-K., 2013. Spatiotemporal variability and long-term trends of ocean acidification in the California Current System. Biogeosci., 10, 193-216. dio: 10.5194/bg-10-193-2013.

Keeling, C. D., 1960. The concentration and isotopic abundances of carbon dioxide in the atmosphere, Tellus XII, 200-203.

Key, R. M., Kozyr, A., Sabine, C. L., Lee, K., Wanninkhof, R., Bullister, J. L., Feely, R. A., Millero, F. J., Mordy, C. and Peng, T.H., 2004. A global ocean carbon climatology: Results from Global Data Analysis Project (GLODAP). Glob. Biogeochem. Cycles, 18 (4): doi. GB4031 DEC 29 2004.

Key, R. M., Tanhua, T., Olsen, A., Hoppema, M., Jutterstrom,S., Schirnick, C., van Heuven, S., Kozyr, A., Lin, X., Wallace, D. W. and Mintrop, L., 2010. The CARINA data synthesis project: introduction and overview. Earth Syst. Sci. Data, 2, 105-121. www.earth-syst-sci-data.net/2/105/2010.

Lee, K., Tong, L. T., Millero, F. J., Sabine, C. L., Dickson, A. G., Goyet, C., Park, G-H., Wanninkhof, R., Feely, R. A. and Key, R. M., 2006. Global relationships of total alkalinity with salinty and temperature in surface watrs of the world's oceans. Geophys. Res. Let. 33, L19605, doi:10.1029/2006GL27207.

Lueker, T. J., Dickson, A. G. and Keeling, C. D., 2000. Ocean pCO_2 calculated from dissolved inorganic carbon, alkalinity and equations K_1 and K_2: validation based on laboratory measurements of CO_2 in gas and seawater at equilibrium. Marine Chem., 70, 105-119.

Marion, G. M., Millero, F. J., Camoes, M. F., Spitzer, P., Feistel,R. and Chen, C.-T. A., 2011. pH of seawater, Marine Chem., 126, 89-96.

Millero, F. J., Lee, K. amd Roche, M., 1998. Distribution of alkalinity in the surface waters of the major oceans. Marine Chem., 60, 111-130.

Mucci, A., 1983. The solubility of calcite and aragonite in seawater at various salinities, temperatures and one atmosphere total pressure. Am. Jour. Sci., 283, 780-799.

NCEP Reanalysis data, 2001. NCEP/NCAR Reanalysis Monthly Means and Other Derived Variables, provided by the NOAA-CIRES Climate Diagnostics Center, Boulder, CO. http://www.cdc.noaa.gov/cdc/data/ncep.reanalysis.derived.html

Olafsson, J., Olafsdottir, S. R., Benoit-Cattin, A., Danielsen, M., Arnarson, T. S., and Takahashi, T., 2009. Rate of Iceland Sea acidification from time series measurements, Biogeosciences, 6, 2661-2668.

Orr, J. C. and 26 coauthors, 2005. Anthropogenic ocean acidification over the twenty-first century and its impact on calcifying organisms. Nature, 437, 681-686. doi: 10.1038/nature04095.

Robbins, L. L., Wynn, J. G., Lisle, J., Yates, K. K., Knorr, P. O., Byrne, R. H., Liu, X., Patsavas, M. C., Azetsu-Scott, K. and Takahashi, T., 2013. Baseline monitoring of the Western Arctic Ocean estimates 20% of the Canadian Basin surface waters are undersaturated with respect to aragonite. PLoS ONE, 8, Issue 9, e73796, 1-15.

Santana-Casiano, J. M., González-Dávila, M., Rueda, M.-J., Llinás, O. and González-Dávila, E.-F., 2007. The interannual variability of oceanic CO_2 parameters in the northeast Atlantic subtropical gyre at the ESTOC site, Global Biogeochem. Cycles, 21, GB1015, doi:10.1029/2006GB002788.

Sjorberg, S., Nordin, N. and Ingri, N., 1981. Equilibrium and structural studies of silicon(IV) and aluminium(III) in aqueous solution. II. Formation constants for the monosilicate ions $SiO(OH)^{3-}$ and $SiO_2(OH)_2^{2-}$. A precision study at 25 ^{o}C in a simplified seawater medium. Marine Chem., 19, 521-532.

Takahashi, T., Olafsson, J., Goddard, J., Chipman, D. W. and Sutherland, S. C., 1993. Seasonal variation of CO_2 and nutrients in the high-latitude surface oceans: A comparative study. Global Biogeochemical Cycles, 7, 843-878.

Takahashi, T., and 28 coauthors, 2009. Climatological mean and decadal changes in surface ocean pCO_2, and net sea-air CO_2 flux over the global oceans. Deep-Sea Res. II, 554-577. doi: 10.1016/j.dsr2.2008.12.009.

Takahashi, T., Sutherland, S. C. and Kozyr, A., 2013. Global Ocean Surface Water Partial Pressure of CO_2 Database: Measurements Performed During 1957–2012 (Version 2012). ORNL/CDIAC-160, NDP-088(V2012). Carbon Dioxide Information Analysis Center, Oak Ridge National Laboratory, U.S. Department of Energy, Oak Ridge, Tennessee, doi: 10.3334/CDIAC/OTG.NDP088(V2012).

Takahashi, T., Sutherland,S. C., Chipman, D. W., Goddard, J. G., Ho, C., Newberger, T., Sweeney, C, and Munro, D. R., 2014. Climatological Distributions of pH, pCO_2, Total CO_2, Alkalinity, and $CaCO_3$ Saturation in the Global Surface Ocean, and Temporal Changes at Selected Locations. Marine Chemistry, 164, 95-125.

Tanhua, T. et al., 2009. CARINA Data Synthesis Project. ORNL/CDIAC-157, NDP-091, Oak Ridge National Laboratory, U. S. Department of Energy, pp. 11.

Walsh, J. J., and 21 coauthors, 1989. Carbon and nitrogen cycling within the Bering/Chukchi Seas: Source regions for organic matter effecting AOU demands of the Arctic Ocean. Prog. Oceanog., 22, 277-359.

Weiss, R. F., 1974. Carbon dioxide in water and seawater: The solubility of a non-ideal gas, Marine Chem., 2, 203-215.

Woodgate, R. A, Aagaard, K. and Weingartner, T. J., 2006. Interannual changes in the Bering Strait fluxes of volume, heat and freshwater between 1991 and 2004. Geophys. Res. Letters, 33, L15609, doi:10.1029/2006GL026931, 2006.